arXiv:cond-mat/9711187v1 [cond-mat.mtrl-sci] 19 Nov 1997

Semiconductor Science and Technology

Review article on:

A review of coherent phenomena in photoexcited semiconductors is presented. In particular, two classes of phenomena are considered: On the one hand the role played by optically-induced phase coherence in the ultrafast spectroscopy of semiconductors; On the other hand the Coulomb-induced effects on the coherent optical response of low-dimensional structures.

All the phenomena discussed in the paper are analyzed in terms of a theoretical framework based on the density-matrix formalism. Due to its generality, this quantum-kinetic approach allows a realistic description of coherent as well as incoherent, i.e. phase-breaking, processes, thus providing quantitative information on the coupled — coherent vs. incoherent— carrier dynamics in photoexcited semiconductors.

The primary goal of the paper is to discuss the concept of quantum-mechanical phase coherence as well as its relevance and implications on semiconductor physics and technology. In particular, we will discuss the dominant role played by optically induced phase coherence on the process of carrier photogeneration and relaxation in bulk systems. We will then review typical field-induced coherent phenomena in semiconductor superlattices such as Bloch oscillations and Wannier-Stark localization. Finally, we will discuss the dominant role played by Coulomb correlation on the linear and non-linear optical spectra of realistic quantum-wire structures.

Coherent phenomena in semiconductors

Fausto Rossi
Istituto Nazionale per la Fisica della Materia (INFM) and
Dipartimento di Fisica, Università di Modena
via Campi 213/A, I-41100 Modena, Italy
E-mail: Rossi@UNIMO.IT

I. INTRODUCTION

The resonant excitation by coherent optical radiation of an electronic transition in a semiconductor, e.g. a valence- to conduction-band excitation, creates a quantum-mechanical coherent superposition of the initial and final states of the transition, called optical polarization. The non-linear optical properties of this coherent superposition, together with its time evolution, can be used to provide a sensitive measurement of many fundamental parameters of the semiconductor material[1] including elastic and inelastic scattering, energy level splittings between nearly degenerate states, energy relaxation, as well as associated information such as Landé g-factors and band-mixing.

In general, non-linear laser spectroscopy is a very established and well understood means to probe these phenomena[2–9]. However, the description of the non-linear optical response of a semiconductor crystal can be considerably more complex than for simple isolated and non-interacting atoms[8]. This is particularly true for the case of the ultrafast optical spectroscopy used for the study of the sub-picosecond dynamics of photoexcited carriers in bulk systems as well as in semiconductor heterostructures[1,10,11].

The life-time of the coherent quantum-mechanical superposition generated by an ultrafast laser excitation, called "dephasing time", determines the typical time-scale on which coherent phenomena can be observed. Such dephasing time reflects the role played by the various "incoherent", i.e. phase-breaking, mechanisms in destroying the phase coherence induced by the laser photoexcitation. Since semiconductors are characterized by very short electron-hole dephasing times, of the order of few hundreds of femtoseconds[8], coherent phenomena manifest themselves only through ultrafast optical experiments with sub-picosecond time resolutions[1]. On this time-scale, the ultrafast evolution of photoexcited electron-hole pairs will reflect the strong coupling between coherent and incoherent dynamics, thus providing invaluable information on the non-equilibrium relaxation processes occurring in the semiconductor, e.g. carrier-carrier and carrier-phonon scattering.

The aim of this paper is to review the basic aspects related to coherent phenomena in semiconductors. In particular, we will focus on the ultrafast —coherent vs. incoherent— carrier dynamics as well as on Coulomb-correlation effects in photoexcited semiconductors.

The paper is organized as follows. In the remainder of this section, after a brief historical account of coherent experiments in solids, we will try to gain more insight into the concept of coherence by introducing a simplified description of the light-matter interaction in terms of a two-level model. In section II we will discuss the theoretical approach commonly used for a realistic description of both coherent and incoherent phenomena in various semiconductor structures, e.g. bulk systems, semiconductor superlattices, quantum wells and wires. Section III deals with ultrafast carrier photoexcitation and relaxation in bulk semiconductors; In particular, we will discuss the dominant role played by coherence on the carrier photogeneration process. In section IV we will review and discuss typical field-induced phenomena in superlattices, namely Bloch oscillations and Wannier-Stark localization, as well as their dephasing dynamics. Section V is devoted to the analysis of the coherent optical response of quasi-one-dimensional systems; More specifically, we will discuss the strong modifications induced by Coulomb correlation on the linear and non-linear optical spectra of realistic quantum-wire structures. Finally, in section VI we will summarize and draw some conclusions.

A. Historical background

Coherent phenomena in atomic and molecular systems have been investigated for a long time[2]. The first spin echo experiment[12] was performed in 1950 on protons in a water solution of Fe^{+++} ions. Pulses in the radio frequency range were generated by means of a gated oscillator with pulse widths between 20 μs and a few milliseconds. With these pulses dephasing times of the order of 10 ms have been measured.

In the 1960s echo experiments were brought into the visible range[13,14]. A Q-switched ruby laser produced pulses of approximately 10 ns duration which were used to observe photon echoes from ruby. In this case the dephasing times were of the order of 100 ns.

As already pointed out, for the observation of any coherent dynamics the pulse width has to be shorter than the typical dephasing time. Since in semiconductors electron-hole dephasing times are much shorter —they are in the range of a few picoseconds down to some femtoseconds—, coherent experiments in semiconductors had to wait until the development of suitable lasers able to generate sub-picosecond pulses.

B. Ultrafast spectroscopy in semiconductors

The physical phenomena governing the ultrafast carrier dynamics in photoexcited semiconductors can be divided into two classes: *coherent phenomena*, i.e. phenomena related to the quantum-mechanical phase coherence induced by the laser photoexcitation, and *incoherent phenomena*, i.e. phenomena induced by the various phase-breaking scattering mechanisms. The above classification in terms of coherent and incoherent phenomena is not purely academic; It corresponds to rather different experimental techniques for the investigation of these two different regimes.

From an historical point of view, the optical spectroscopy in semiconductors started with the analysis of relatively slow incoherent phenomena (compared to the electron-hole dephasing time-scale). The investigation of nonequilibrium carriers started with the analysis of the incoherent energy-relaxation processes in the late 1960s using cw-lasers[15]. In the 1970s pulse sources for the study of photoexcited carriers became available[16] and this initiated time-resolved studies of the energy-relaxation process. Many experiments based on different techniques have been performed[1]: band-to-band luminescence[17,18] which monitors the product of electron and hole distribution functions, band-to-acceptor luminescence[19–21] which provides information on the electron distribution functions only, and pump-and-probe measurements[22–26] where the measured differential transmission is proportional to the sum of electron and hole distribution functions.

The theoretical analysis of these relaxation phenomena is commonly based on the semiclassical Boltzmann theory. The Boltzmann equations for both electron and hole distribution functions are commonly solved by means of semiclassical Monte Carlo simulations[27–29].

In addition to the analysis of incoherent energy-relaxation processes, the ultrafast optical spectroscopy has allowed the investigation of coherent phenomena. As already pointed out, a coherent laser field creates, in addition to a non-equilibrium carrier distribution, a coherent polarization. The investigation of the coherent dynamics in semiconductors started in the 1980s. Different aspects have been investigated[1]: the optical Stark effect[30–33], the dephasing of free carriers[34] and excitons[35–37], quantum beats related to various types of level splittings[38–41], charge oscillations in double-quantum-well systems[42,43] and superlattices[44], many-particle effects[45–48], and the emission of coherent THz radiation[49,50].

These experiments cannot be analyzed within the framework of the Boltzmann equation. The reason is that this coherent polarization reflects a well-defined phase relation between electrons and holes, which is neglected within the semiclassical Boltzmann theory. Any proper description requires a quantum-mechanical treatment where, in addition to the distribution functions of electrons and holes, also the interband polarization is taken into account as an independent variable. Several approaches have been used in the literature[8]: Bogoliubov transformations[51], nonequilibrium Green's functions[52–56], band-edge equations based on the real-space density matrix[57], and the density matrix formalism in momentum space[58–64].

During the last decade the time resolution has been further improved down to few tens of femtoseconds[65]. On such extremely short time-scale coherent effects can no longer be neglected and are found to play a dominant role also for the case of typical incoherent measurements such as time-resolved and time-integrated luminescence. In such conditions, the carrier dynamics is the result of a strong interplay between coherent and incoherent phenomena. Therefore, the traditional separation [1]

---

[1] From an historical point of view, the theoretical approaches commonly used for the interpretation of coherent phenomena provide a rather qualitative description of phase-breaking processes in terms of phenomenological energy-relaxation and dephasing rates. On the other hand, incoherent phenomena were traditionally investigated in terms of semiclassical Monte Carlo simulations, which provide a microscopic description of the

between coherent and incoherent approaches for the theoretical investigation of photoexcited semiconductors is no longer valid. What is needed is a comprehensive theoretical framework able to describe on the same kinetic level both classes of phenomena as well as their mutual coupling. To this purpose, a generalized Monte Carlo method for the analysis of both coherent and incoherent phenomena has been recently proposed[66–70]. The spirit of the method is to combine the advantages of the conventional Monte Carlo approach[27–29] in treating the incoherent, i.e. phase-breaking, dynamics with the strength of a quantum-kinetic approach in describing coherent phenomena[8]. In particular, the coherent contributions are evaluated by means of a direct numerical integration while the incoherent ones are "sampled" by means of a conventional Monte Carlo simulation in the three-dimensional **k**-space.

This theoretical approach has ben applied successfully to the analysis of various ultrafast optical experiments, e.g. four-wave-mixing studies of many-body effects in bulk GaAs[71,72] and luminescence studies of the hot-carrier photogeneration process[73–75].

C. The meaning of coherence

In order to clarify the concept of phase coherence, let us consider the simplest physical model for the description of light-matter interaction, i.e. an optically driven two-level system[1,2]. Within a two-level picture, a ground state a with energy ϵ_a and an excited state b with energy ϵ_b are mutually coupled by a driving force, e.g. an external field, and/or by their mutual interaction, e.g. Coulomb correlation. The two-level-system Hamiltonian

$$\mathbf{H} = \mathbf{H}_\circ + \mathbf{H}' \tag{1}$$

is the sum of a free-level contribution

$$\mathbf{H}_\circ = \epsilon_a a_a^\dagger a_a + \epsilon_b a_b^\dagger a_b \tag{2}$$

and of a coupling term

$$\mathbf{H}' = U_{ba} a_b^\dagger a_a + U_{ab} a_a^\dagger a_b \ . \tag{3}$$

Here, the usual second-quantization picture in terms of creation ($a^\dagger$) and destruction (a) operators has been introduced[8]. The two terms forming the coupling Hamiltonian $\mathbf{H}'$ will induce transitions from state a to b and vice versa according to the coupling constant $U_{ba} = U_{ab}^*$.

As a starting point, let us consider a single-electron system. In the absence of interlevel coupling ($U_{ab} = 0$), we have two stationary states,

$$|a(t)\rangle = exp\left(-\frac{i\epsilon_a t}{\hbar}\right) a_a^\dagger |0\rangle \ , \qquad |b(t)\rangle = exp\left(-\frac{i\epsilon_b t}{\hbar}\right) a_b^\dagger |0\rangle \tag{4}$$

($|0\rangle$ being the vacuum state), corresponding to a single electron in level a or b, respectively. On the contrary, in the presence of interlevel coupling, the state of the system is, in general, a linear superposition of the non-interacting states in equation (4):

$$|\psi(t)\rangle = c_a(t)|a(t)\rangle + c_b(t)|b(t)\rangle \ , \tag{5}$$

whose coefficients obey the following equations of motion:

$$\begin{aligned} \frac{d}{dt}c_a &= \frac{U_{ab}}{i\hbar} exp\left(\frac{i(\epsilon_a - \epsilon_b)t}{\hbar}\right) c_b \\ \frac{d}{dt}c_b &= \frac{U_{ba}}{i\hbar} exp\left(\frac{i(\epsilon_b - \epsilon_a)t}{\hbar}\right) c_a \ . \end{aligned} \tag{6}$$

Again, we see that in the absence of interlevel coupling ($U = 0$) there is no time variation of the coefficients, i.e. if the system is prepared in state $|a\rangle$ or $|b\rangle$ it will remain in such eigenstate. On the contrary, the interlevel coupling induces a time variation of the coefficients.

---

non-equilibrium scattering dynamics.

The above two-level model provides the simplest description of light-matter interaction in atomic and molecular systems[2] as well as in solids[8]. The coupling term in equation (3) has the same structure of a field-dipole interaction Hamiltonian and the driving force u can be regarded as a coherent light field. We will now consider two limiting cases: the ultrashort- and continuous-excitation regimes.

An ultrashort optical excitation can be described in terms of a delta-like light pulse: $U_{ab}(t) = \eta\delta(t)$. In this case, the equations of motion (6) can be solved analytically: Due to this excitation, the two-level system will undergo an instantaneous transition from its ground state $\{c_a = 1, c_b = 0\}$ to the excited state $\{c_a = \cos\alpha, c_b = -i\sin\alpha\}$, with $\alpha = \frac{\eta}{\hbar}$. Therefore, after the pulse the system will remain in the excited state

$$|\psi(t)\rangle = (\cos\alpha)|a(t)\rangle + (-i\sin\alpha)|b(t)\rangle \ , \tag{7}$$

which is a coherent quantum-mechanical superposition of the two non-interacting states. In addition to a finite occupation probability $|c_b|^2 = sin^2\alpha$ of the excited state, there exists a well defined phase coherence between the ground- and the excited-state contributions, i.e. a part from their amplitudes, the coefficients c_a and c_b differ in phase by $\frac{\pi}{2}$. This is what is generally meant by optically induced phase coherence.

Let us now consider a continuous optical excitation resonant with our two-level system: $U_{ab}(t) = U_\circ e^{i\omega_L t}$ with $\hbar\omega_L = \epsilon_b - \epsilon_a$. Also for this case, equations (6) can be solved analytically. In particular, for the initial condition at $t = 0$ given by the ground state $\{c_a = 1, c_b = 0\}$, the solution is given by

$$|\psi(t)\rangle = \cos(\frac{1}{2}\omega_R t)|a(t)\rangle - i\sin(\frac{1}{2}\omega_R t)|b(t)\rangle \ , \tag{8}$$

where $\omega_R = \frac{2U_\circ}{\hbar}$ is the so-called Rabi frequency. Compared to the previous case, the continuous excitation gives rise to a periodic population and depopulation of the excited state according to $|c_b|^2 = sin^2(\frac{1}{2}\omega_R t)$. This purely coherent phenomenon is known as "Rabi-oscillation regime". As for the previous case, the excited state in equation (8) reflects a well-defined optically-induced phase coherence.

As mentioned above, the interlevel-coupling Hamiltonian in equation (3) may also describe, in addition to an optical excitation, some interlevel coupling due, e.g. to Coulomb interaction. Also in this case, in the presence of this interlevel coupling the quantum state of the system will result in a coherent superposition of the two stationary states in (4). Again, this coupling will induce a well-defined phase coherence between the two levels.

From the above considerations we see that coherent phenomena can be divided into two basic classes: *optically-induced* and *Coulomb-induced* phenomena. In order to describe the optical response of an electron gas within a semiconductor crystal, the above analysis, based on a single two-level system, has to be replaced by a statistical-ensemble approach, i.e. a description based on a collection of independent two-level systems. Any statistical ensemble of quantum systems is properly described by its single-particle density matrix[64]

$$\rho_{nn'} = \langle a^\dagger_{n'} a_n \rangle \ , \tag{9}$$

where n denotes a generic set of quantum numbers. Its diagonal elements $f_n = \rho_{nn}$ provide the average occupation numbers while the non-diagonal terms describe the degree of phase coherence between states n and n'. For the case of our two-level system, $\rho_{nn'}$ reduces to a two-by-two matrix: the diagonal elements $f_a = \rho_{aa}$ and $f_b = \rho_{bb}$ describe, respectively, the average occupation of levels a and b, while the non-diagonal terms $p = \rho_{ba}$ and $p^* = \rho_{ab}$ reflect the average degree of phase coherence between the ground and the excited state. Starting from the Heisenberg equations of motion for the creation and destruction operators, i.e.

$$i\hbar\frac{d}{dt}a^\dagger_n = [a^\dagger_n, \mathbf{H}] \ , \qquad i\hbar\frac{d}{dt}a_n = [a_n, \mathbf{H}] \ , \tag{10}$$

we obtain the following equations of motion for the above density-matrix elements:

$$\begin{aligned} \frac{d}{dt}f_b &= -\frac{d}{dt}f_a = \frac{2}{\hbar}\Re\left(iU_{ab}p\right) \\ \frac{d}{dt}p &= \frac{\epsilon_b - \epsilon_a}{i\hbar}p + \frac{U_{ba}}{i\hbar}(f_a - f_b) \ . \end{aligned} \tag{11}$$

They are known as optical Bloch equations[1,8] in analogy with the equations first derived by Bloch[76] for the spin systems. This statistical-ensemble description reduces to the previous one for the case of a so

called "pure state", i.e. the case in which all the two-level systems forming the ensemble are in the same quantum-mechanical state $|\psi\rangle$. In this case, the above set of kinetic equations and the equations of motion (6) are totally equivalent. However, as we will discuss in section II, the density-matrix approach introduced so far allows, in addition to the study of coherent phenomena, the analysis of incoherent phenomena, which is not possible within a simple Schrödinger-equation formalism.

The optical Bloch equations (10) provide the simplest description of light-matter interaction. Let us consider again the case of a continuous optical excitation resonant with our two-level system: $U_{ab}(t) = U_\circ e^{i\omega_L t}$. If we choose as initial condition at time $t = 0$ the state $\{f_a = f_\circ, f_b = 0, p = 0\}$, the solution of the above optical Bloch equations is given by:

$$\begin{aligned} f_a(t) &= f_\circ \cos^2(\frac{1}{2}\omega_R t) \\ f_b(t) &= f_\circ \sin^2(\frac{1}{2}\omega_R t) \\ p(t) &= \frac{f_\circ}{4}\left[e^{-i\omega^+ t} - e^{-i\omega^- t}\right] , \end{aligned} \tag{12}$$

where $\omega^\pm = \omega_L \pm \omega_R$. As for the case of a single two-level system, the above solution describes a Rabi-oscillation regime. In particular, the interlevel density-matrix element p originates from the superposition of the two frequency components ω^+ and ω^-. They differ from ω_L by the Rabi frequency ω_R. Such modification of the two-level frequency ω_L due to its coupling with the external field is known as "Rabi splitting"[6].

If we now rewrite the interlevel density-matrix element p in (12) as

$$p(t) = -\frac{if_\circ}{2} e^{-i\omega_L t} \sin(\omega_R t) , \tag{13}$$

we see that, a part from the quantum-mechanical phase factor corresponding to the energy separation $\hbar\omega_L = \epsilon_b - \epsilon_a$, its amplitude exhibits Rabi oscillations according to $\sin(\omega_R t)$. More specifically, we obtain:

$$|p|^2 \propto \sin^2(\omega_R t) \propto \cos^2(\frac{1}{2}\omega_R t)\sin^2(\frac{1}{2}\omega_R t) \propto f_a(t) f_b(t) , \tag{14}$$

i.e. the quantity $|p|^2$ is proportional to the product of the two occupation numbers, thus reflecting the total (or macroscopic) dipole moment of the two-level system at time t. This elucidates the link between optically-induced phase coherence and polarization: a coherent optical excitation gives rise to a coherent quantum-mechanical superposition of the two states which results in a macroscopic polarization of the system. Such polarization field is fully described by the non-diagonal matrix element p in (12).

The above simplified description of light-matter interaction neglects any kind of incoherent, i.e. phase-breaking, phenomena. As we will see in section II, such dephasing processes will lead to a decay of the interband polarization p, thus destroying the optically induced phase coherence in the carrier system.

As a final remark, let us discuss the concept of phase coherence in connection with the choice of representation. On the basis of the density-matrix formalism considered so far, the phase coherence is described by the non-diagonal density-matrix elements $\rho_{nn'}$ in (9). However, this separation in *diagonal* and *non-diagonal* terms is clearly representation dependent: what is diagonal in a given basis is in general not diagonal in a different basis and vice versa. If one considers, as basis set, the eigenstates of the total Hamiltonian $\mathbf{H}$ (which includes the external driving force), the density matrix ρ in (9) is always diagonal, i.e. no phase coherence. Thus, in order to speak of phase coherence, we need to regard the total Hamiltonian $\mathbf{H}$ as the sum of the system Hamiltonian $\mathbf{H}_\circ$ plus a driving-force term $\mathbf{H}'$ (see equation (1)). Provided such separation between *system of interest* and *driving force*, the non-diagonal density-matrix elements within the representation given by the eigenstates of $\mathbf{H}_\circ$ will describe the degree of coherence induced in the system by the driving force $\mathbf{H}'$.

Two typical cases, discussed respectively in sections IV and V, may help in clarifying the meaning of coherence. The first case is that of a semiconductor superlattice in the presence of a constant and homogeneous electric field: As we will see, within the Wannier-Stark representation the Bloch-oscillation dynamics is the result of phase coherence between the various Wannier-Stark states; On the contrary, within the Bloch representation the same phenomenon is purely described in terms of carrier populations, i.e. no off-diagonal density-matrix elements. The second case is that of Coulomb-induced phase coherence: Within a free-particle representation, even at the simplest Hartree-Fock level, Coulomb interaction induces phase coherence between free-carrier states. This is clearly not the case within an exciton basis, where the density matrix is diagonal.

II. THEORETICAL BACKGROUND

In this section we will review in a systematic way the basic ideas used in the theoretical analysis of ultrafast carrier dynamics in semiconductors. The approach we are going to present is based on the density-matrix formalism introduced in section I C.

A. Physical system

In order to study the optical and transport properties of semiconductor bulk and heterostructures, let us consider a gas of carriers in a crystal under the action of an applied electromagnetic field. The carriers will experience their mutual interaction as well as the interaction with the phonon modes of the crystal. Such physical system can be described by the following Hamiltonian:

$$\mathbf{H} = \mathbf{H}_c + \mathbf{H}_p + \mathbf{H}_{cc} + \mathbf{H}_{cp} + \mathbf{H}_{pp} \ . \tag{15}$$

The first term describes the noninteracting-carrier system in the presence of the external electromagnetic field while the second one refers to the free-phonon system. The last three terms describe many-body contributions: they refer, respectively, to carrier-carrier, carrier-phonon, and phonon-phonon interactions.

In order to discuss their explicit form, let us introduce the usual second-quantization field operators $\mathbf{\Psi}^\dagger(\mathbf{r})$ and $\mathbf{\Psi}(\mathbf{r})$. They describe, respectively, the creation and the destruction of a carrier in $\mathbf{r}$. In terms of the above field operators the carrier Hamiltonian $\mathbf{H}_c$ can be written as

$$\mathbf{H}_c = \int d\mathbf{r} \mathbf{\Psi}^\dagger(\mathbf{r}) \left[\frac{\left(-i\hbar\nabla_{\mathbf{r}} - \frac{e}{c}\mathbf{A}(\mathbf{r},t)\right)^2}{2m_\circ} + e\varphi(\mathbf{r},t) + V^l(\mathbf{r}) \right] \mathbf{\Psi}(\mathbf{r}) \ . \tag{16}$$

Here, $V^l(\mathbf{r})$ denotes the periodic potential due to the perfect crystal while $\mathbf{A}(\mathbf{r},t)$ and $\varphi(\mathbf{r},t)$ denote, respectively, the vector and scalar potentials corresponding to the external electromagnetic field. Since we are interested in the electrooptical properties as well as in the ultrafast dynamics of photoexcited carriers, the electromagnetic field acting on the crystal —and the corresponding electromagnetic potentials— will be the sum of two different contributions: the high-frequency laser field responsible for the ultrafast optical excitation and the additional electromagnetic field acting on the photoexcited carriers on a longer time-scale. More specifically, by denoting with the labels 1 and 2 these two contributions, we can write

$$\mathbf{A}(\mathbf{r},t) = \mathbf{A}_1(\mathbf{r},t) + \mathbf{A}_2(\mathbf{r},t) \ , \qquad \varphi(\mathbf{r},t) = \varphi_1(\mathbf{r},t) + \varphi_2(\mathbf{r},t) \tag{17}$$

and recalling that

$$\mathbf{E}(\mathbf{r},t) = -\frac{1}{c}\frac{\partial}{\partial t}\mathbf{A}(\mathbf{r},t) - \nabla_{\mathbf{r}}\varphi(\mathbf{r},t) \ , \qquad \mathbf{B}(\mathbf{r},t) = \nabla_{\mathbf{r}} \times \mathbf{A}(\mathbf{r},t) \tag{18}$$

we have

$$\mathbf{E}(\mathbf{r},t) = \mathbf{E}_1(\mathbf{r},t) + \mathbf{E}_2(\mathbf{r},t) \ , \qquad \mathbf{B}(\mathbf{r},t) = \mathbf{B}_1(\mathbf{r},t) + \mathbf{B}_2(\mathbf{r},t) \ . \tag{19}$$

Equation (18), which gives the electromagnetic fields in terms of the corresponding vector and scalar potentials, reflects the well known gauge freedom: there is an infinite number of possible combinations of $\mathbf{A}$ and φ which give rise to the same electromagnetic field $\{\mathbf{E},\mathbf{B}\}$. We will use such freedom of choice for the laser field (term 1): we assume a homogeneous (space-independent) laser field $\mathbf{E}_1(t)$ fully described by the scalar potential

$$\varphi_1(\mathbf{r},t) = -\mathbf{E}_1(t)\cdot\mathbf{r} \ . \tag{20}$$

This assumption, which corresponds to the well known dipole approximation, is well justified as long as the space-scale of interest is small compared to the light wavelength. The explicit form of the laser field considered here is

$$E_1(t) = E^+(t) + E^-(t) = E_\circ(t)e^{i\omega_L t} + E_\circ^*(t)e^{-i\omega_L t} \ , \tag{21}$$

where $E_\circ(t)$ is the amplitude of the light field and ω_L denotes its central frequency.

With this particular choice of the electromagnetic potentials describing the laser field, the Hamiltonian in (16) can be rewritten as

$$\mathbf{H}_c = \mathbf{H}_c^\circ + \mathbf{H}_{cl} \ , \tag{22}$$

where

$$\mathbf{H}_c^\circ = \int d\mathbf{r} \mathbf{\Psi}^\dagger(\mathbf{r}) \left[\frac{\left(-i\hbar\nabla_{\mathbf{r}} - \frac{e}{c}\mathbf{A}_2(\mathbf{r},t)\right)^2}{2m_\circ} + e\varphi_2(\mathbf{r},t) + V^l(\mathbf{r}) \right] \mathbf{\Psi}(\mathbf{r}) \tag{23}$$

describes the carrier system in the crystal under the action of the electromagnetic field 2 only, while

$$\mathbf{H}_{cl} = e \int d\mathbf{r} \mathbf{\Psi}^\dagger(\mathbf{r}) \varphi_1(\mathbf{r},t) \mathbf{\Psi}(\mathbf{r}) \tag{24}$$

describes the carrier-light (cl) interaction due to the laser photoexcitation.

In analogy with the carrier system, by denoting with $b^\dagger_{\mathbf{q},\lambda}$ and $b_{\mathbf{q},\lambda}$ the creation and destruction operators for a phonon of mode λ and wavevector $\mathbf{q}$, the free-phonon Hamiltonian takes the form

$$\mathbf{H}_p = \sum_{\mathbf{q}\lambda} \hbar\omega_{\mathbf{q}\lambda} b^\dagger_{\mathbf{q}\lambda} b_{\mathbf{q}\lambda} \ , \tag{25}$$

where $\omega_{\mathbf{q}\lambda}$ is the dispersion relation for the phonon mode λ.

Let us now discuss the explicit form of the many-body contributions. The carrier-carrier interaction is described by the two-body Hamiltonian

$$\mathbf{H}_{cc} = \frac{1}{2} \int d\mathbf{r} \int d\mathbf{r}' \mathbf{\Psi}^\dagger(\mathbf{r}) \mathbf{\Psi}^\dagger(\mathbf{r}') V_{cc}(\mathbf{r}-\mathbf{r}') \mathbf{\Psi}(\mathbf{r}') \mathbf{\Psi}(\mathbf{r}) \ , \tag{26}$$

where V_{cc} denotes the Coulomb potential.

Let us now introduce the carrier-phonon interaction Hamiltonian

$$\mathbf{H}_{cp} = \int d\mathbf{r} \mathbf{\Psi}^\dagger(\mathbf{r}) V_{cp}(\mathbf{r}) \mathbf{\Psi}(\mathbf{r}) \ , \tag{27}$$

where

$$V_{cp} = \sum_{\mathbf{q}\lambda} \left[\tilde{g}_{\mathbf{q}\lambda} b_{\mathbf{q}\lambda} e^{i\mathbf{q}\cdot\mathbf{r}} + \tilde{g}^*_{\mathbf{q}\lambda} b^\dagger_{\mathbf{q}\lambda} e^{-i\mathbf{q}\cdot\mathbf{r}} \right] \tag{28}$$

is the electrostatic phonon potential induced by the lattice vibrations. Here, the explicit form of the coupling function $\tilde{g}_{\mathbf{q}\lambda}$ depends on the particular phonon mode λ (acoustic, optical, etc.) as well as on the coupling mechanism considered (deformation potential, polar coupling, etc.).

Let us finally discuss the phonon-phonon contribution $\mathbf{H}_{pp}$. The free-phonon Hamiltonian $\mathbf{H}_p$ in (25), which describes a system of noninteracting phonons, by definition accounts only for the harmonic part of the lattice potential. However, non-harmonic contributions of the interatomic potential can play an important role in determining the lattice dynamics in highly excited systems[77], since they are responsible for the decay of optical phonons into phonons of lower frequency. In our second-quantization picture, these non-harmonic contributions can be described in terms of a phonon-phonon interaction which induces, in general, transitions between free-phonon states. Here, we will not discuss the explicit form of the phonon-phonon Hamiltonian $\mathbf{H}_{pp}$ responsible for such a decay. We will simply assume that such phonon-phonon interaction is so efficient to maintain the phonon system in thermal equilibrium. This corresponds to neglecting hot-phonon effects[78].

It is well known that the coordinate representation used so far is not the most convenient one in describing the electron dynamics within a periodic crystal. In general, it is more convenient to employ the representation given by the eigenstates of the noninteracting-carrier Hamiltonian —or a part of it— since it automatically accounts for some of the symmetries of the system. For the moment we will simply consider an orthonormal basis set $\{\phi_n(\mathbf{r})\}$ without specifying which part of the Hamiltonian is diagonal in such representation. This will allow us to write down equations valid in any quantum-mechanical representation. Since the noninteracting-carrier Hamiltonian is, in general, a function of

time, also the basis functions ϕ_n may be time-dependent. Here, the label n denotes, in general, a set of discrete and/or continuous quantum numbers. In the absence of electromagnetic field, the above wavefunctions will correspond to the well known Bloch states of the crystal and the index n will reduce to the wavevector $\mathbf{k}$ plus the band (or subband) index ν. In the presence of a homogeneous magnetic field the eigenfunctions ϕ_n may instead correspond to Landau states. Finally, for the case of a constant and homogeneous electric field, there exist two equivalent representations: the accelerated Bloch states and the Wannier-Stark picture. Such equivalence results to be of crucial importance in understanding the relationship between Bloch oscillations and Wannier-Stark localization and, for this reason, it will be discussed in more detail in section IV A.

Let us now reconsider the system Hamiltonian introduced so far in terms of such ϕ_n representation. As a starting point, we may expand the second-quantization field operators in terms of the new wavefunctions:

$$\mathbf{\Psi}(\mathbf{r}) = \sum_n \phi_n(\mathbf{r}) a_n \ , \qquad \mathbf{\Psi}^\dagger(\mathbf{r}) = \sum_n \phi_n^*(\mathbf{r}) a_n^\dagger \ . \tag{29}$$

The above expansion defines the new set of second-quantization operators $a_n^\dagger$ and a_n; They describe, respectively, the creation and destruction of a carrier in state n.

For the case of a semiconductor structure (the only one considered here), the energy spectrum of the noninteracting-carrier Hamiltonian (23) —or a part of it— is always characterized by two well-separated energy regions: the valence and the conduction band. Also in the presence of an applied electromagnetic field, the periodic lattice potential V^l gives rise to a large energy gap. Therefore, we deal with two energetically well-separated regions, which suggests the introduction of the usual electron-hole picture. This corresponds to a separation of the set of states $\{\phi_n\}$ into conduction states $\{\phi_i^e\}$ and valence states $\{\phi_j^h\}$. Thus, also the creation (destruction) operators $a_n^\dagger$ (a_n) introduced in equation (29) will be divided into creation (destruction) electron and hole operators: $c_i^\dagger$ (c_i) and $d_j^\dagger$ (d_j). In terms of the new electron-hole picture, the expansion (29) is given by:

$$\begin{aligned} \mathbf{\Psi}(\mathbf{r}) &= \sum_i \phi_i^e(\mathbf{r}) c_i + \sum_j \phi_j^{h*}(\mathbf{r}) d_j^\dagger \\ \mathbf{\Psi}^\dagger(\mathbf{r}) &= \sum_i \phi_i^{e*}(\mathbf{r}) c_i^\dagger + \sum_j \phi_j^h(\mathbf{r}) d_j \ . \end{aligned} \tag{30}$$

If we now insert the above expansion into equation (23), the noninteracting-carrier Hamiltonian takes the form

$$\mathbf{H}_c^\circ = \sum_{ii'} \epsilon_{ii'}^e c_i^\dagger c_{i'} + \sum_{jj'} \epsilon_{jj'}^h d_j^\dagger d_{j'} = \mathbf{H}_e^\circ + \mathbf{H}_h^\circ \ , \tag{31}$$

where

$$\epsilon_{ll'}^{e/h} = \pm \int d\mathbf{r} \phi_l^{e/h*}(\mathbf{r}) \left[\frac{\left(-i\hbar\nabla_{\mathbf{r}} - \frac{e}{c}\mathbf{A}_2\right)^2}{2m_\circ} + e\varphi_2 + V^l - \epsilon_\circ \right] \phi_{l'}^{e/h}(\mathbf{r}) \tag{32}$$

are just the matrix elements of the Hamiltonian in the ϕ-representation. The $\pm$ sign refers, respectively, to electrons and holes while $\epsilon_\circ$ denotes the conduction-band edge. Here, we neglect any valence-to-conduction band coupling due to the external electromagnetic field and vice versa. This is well fulfilled for the systems and field-regimes we are going to discuss in this paper. As already pointed out, the above Hamiltonian may be time-dependent. We will discuss this aspect in the following section, where we will derive our set of kinetic equations.

Let us now write in terms of our electron-hole representation the carrier-light interaction Hamiltonian (24):

$$\mathbf{H}_{cl} = -\sum_{i,j} \left[\mu_{ij}^{eh} E^-(t) c_i^\dagger d_j^\dagger + \mu_{ij}^{eh*} E^+(t) d_j c_i \right] \ . \tag{33}$$

The above expression has been obtained within the well known rotating-wave approximation[8] by neglecting intraband transitions, absent for the case of optical excitations. Here, μ_{ij}^{eh} denotes the optical dipole matrix element between states ϕ_i^e and ϕ_j^h.

Similarly, the carrier-carrier Hamiltonian (26) can be rewritten as:

$$\begin{aligned}\mathbf{H}_{cc} = & \frac{1}{2}\sum_{i_1 i_2 i_3 i_4} V^{cc}_{i_1 i_2 i_3 i_4} c^\dagger_{i_1} c^\dagger_{i_2} c_{i_3} c_{i_4} \\ & + \frac{1}{2}\sum_{j_1 j_2 j_3 j_4} V^{cc}_{j_1 j_2 j_3 j_4} d^\dagger_{j_1} d^\dagger_{j_2} d_{j_3} d_{j_4} \\ & - \sum_{i_1 i_2 j_1 j_2} V^{cc}_{i_1 j_1 j_2 i_2} c^\dagger_{i_1} d^\dagger_{j_1} d_{j_2} c_{i_2},\end{aligned} \tag{34}$$

where

$$V^{cc}_{l_1 l_2 l_3 l_4} = \int d\mathbf{r} \int d\mathbf{r}' \phi^*_{l_1}(\mathbf{r}) \phi^*_{l_2}(\mathbf{r}') V^{cc}(\mathbf{r}-\mathbf{r}') \phi_{l_3}(\mathbf{r}') \phi_{l_4}(\mathbf{r}) \tag{35}$$

are the Coulomb matrix elements within our ϕ-representation. The first two terms describe the repulsive electron-electron and hole-hole interaction while the last one describes the attractive electron-hole interaction. Here, we neglect terms that do not conserve the number of electron-hole pairs, i.e. impact-ionization and Auger-recombination processes[79], as well as the interband exchange interaction. This monopole-monopole approximation is justified as long as the exciton binding energy is small compared to the energy gap.

Finally, let us rewrite the carrier-phonon interaction Hamiltonian introduced in equation (27):

$$\begin{aligned}\mathbf{H}_{cp} = & \sum_{ii',\mathbf{q}\lambda} \left[g^e_{ii',\mathbf{q}\lambda} c^\dagger_i b_{\mathbf{q}\lambda} c_{i'} + g^{e*}_{ii',\mathbf{q}\lambda} c^\dagger_{i'} b^\dagger_{\mathbf{q}\lambda} c_i \right] \\ & - \sum_{jj',\mathbf{q}\lambda} \left[g^h_{jj',\mathbf{q}\lambda} d^\dagger_j b_{\mathbf{q}\lambda} d_{j'} + g^{h*}_{jj',\mathbf{q}\lambda} d^\dagger_{j'} b^\dagger_{\mathbf{q}\lambda} d_j \right]\end{aligned} \tag{36}$$

with

$$g^{e/h}_{ll',\mathbf{q}\lambda} = \tilde{g}_{\mathbf{q}\lambda} \int d\mathbf{r} \phi^{e/h*}_l(\mathbf{r}) e^{i\mathbf{q}\cdot\mathbf{r}} \phi^{e/h}_{l'}(\mathbf{r}) \ . \tag{37}$$

In equation (36) we can clearly recognize four different contributions corresponding to electron and hole phonon absorption and emission.

B. Kinetic description

Our kinetic description of the ultrafast carrier dynamics in semiconductors is based on the density-matrix formalism introduced in section I C. Since this approach has been reviewed and discussed in several papers[64,80] and text-books[1,8], here we will simply recall in our notation the kinetic equations relevant for the analysis of carrier dynamics in semiconductor heterostructures, generalizing the approach presented in[64] to the case of a time-dependent quantum-mechanical representation.

The set of kinetic variables is the same considered in[64]. Given our electron-hole representation $\{\phi^e_i\}, \{\phi^h_j\}$, we will consider the intraband electron and hole single-particle density matrices

$$f^e_{ii'} = \left\langle c^\dagger_i c_{i'} \right\rangle \ , \qquad f^h_{jj'} = \left\langle d^\dagger_j d_{j'} \right\rangle \tag{38}$$

as well as the corresponding interband density matrix

$$p_{ji} = \left\langle d_j c_i \right\rangle \ . \tag{39}$$

Here, the diagonal elements f^e_{ii} and f^h_{jj} correspond to the electron and hole distribution functions of the Boltzmann theory while the non-diagonal terms describe intraband polarizations. On the contrary, the interband density-matrix elements p_{ji} describe interband (or optical) polarizations.

In order to derive the set of kinetic equations, i.e. the equations of motion for the above kinetic variables, the standard procedure starts by deriving the equations of motion for the electron and hole operators introduced in (30):

$$c_i = \int d\mathbf{r}\phi_i^{e*}(\mathbf{r})\mathbf{\Psi}(\mathbf{r}) \ , \qquad d_j = \int d\mathbf{r}\phi_j^{h*}(\mathbf{r})\mathbf{\Psi}^\dagger(\mathbf{r}) \ . \tag{40}$$

By applying the Heisenberg equation of motion for the field operator $\mathbf{\Psi}$, i.e.

$$\frac{d}{dt}\mathbf{\Psi} = \frac{1}{i\hbar}\left[\mathbf{\Psi}, \mathbf{H}\right] \ , \tag{41}$$

it is easy to obtain the following equations of motion:

$$\begin{aligned}
\frac{d}{dt}c_i &= \frac{1}{i\hbar}\left[c_i, \mathbf{H}\right] + \frac{1}{i\hbar}\sum_{i'} Z^e_{ii'}c_{i'} \\
\frac{d}{dt}d_j &= \frac{1}{i\hbar}\left[d_j, \mathbf{H}\right] + \frac{1}{i\hbar}\sum_{j'} Z^h_{jj'}d_{j'}
\end{aligned} \tag{42}$$

with

$$Z^{e/h}_{ll'} = i\hbar\int d\mathbf{r}\left(\frac{d}{dt}\phi_l^{e/h*}(\mathbf{r})\right)\phi_{l'}^{e/h}(\mathbf{r}) \ . \tag{43}$$

As for the case of equation (31), here we neglect again valence-to-conduction band coupling and vice versa. Compared to the more conventional Heisenberg equations of motion, they contain an extra-term, the last one. It accounts for the possible time dependence of our ϕ-representation which will induce transitions between different states according to the matrix elements $Z_{ll'}$.

By combining the above equations of motion with the definitions of the kinetic variables in (38-39), the resulting set of kinetic equations can be schematically written as:

$$\begin{aligned}
\frac{d}{dt}f^e_{i_1i_2} &= \frac{d}{dt}f^e_{i_1i_2}\bigg|_{\mathbf{H}} + \frac{d}{dt}f^e_{i_1i_2}\bigg|_{\phi} \\
\frac{d}{dt}f^h_{j_1j_2} &= \frac{d}{dt}f^h_{j_1j_2}\bigg|_{\mathbf{H}} + \frac{d}{dt}f^h_{j_1j_2}\bigg|_{\phi} \\
\frac{d}{dt}p_{j_1i_1} &= \frac{d}{dt}p_{j_1i_1}\bigg|_{\mathbf{H}} + \frac{d}{dt}p_{j_1i_1}\bigg|_{\phi} \ .
\end{aligned} \tag{44}$$

They exhibit the same structure of the equations of motion (42) for the electron and hole creation and destruction operators: a first term induced by the system Hamiltonian $\mathbf{H}$ (which does not account for the time variation of the basis states) and a second one induced by the time dependence of the basis functions ϕ.

Let us start discussing this second term, whose explicit form is:

$$\begin{aligned}
\frac{d}{dt}f^e_{i_1i_2}\bigg|_{\phi} &= \frac{1}{i\hbar}\sum_{i_3i_4}\left[Z^e_{i_2i_4}\delta_{i_1i_3} - Z^e_{i_3i_1}\delta_{i_2i_4}\right]f^e_{i_3i_4} \\
\frac{d}{dt}f^h_{j_1j_2}\bigg|_{\phi} &= \frac{1}{i\hbar}\sum_{j_3j_4}\left[Z^h_{j_2j_4}\delta_{j_1j_3} - Z^h_{j_3j_1}\delta_{j_2j_4}\right]f^h_{j_3j_4} \\
\frac{d}{dt}p_{j_1i_1}\bigg|_{\phi} &= \frac{1}{i\hbar}\sum_{i_2j_2}\left[Z^h_{j_1j_2}\delta_{i_1i_2} + Z^e_{i_1i_2}\delta_{j_1j_2}\right]p_{j_2i_2} \ .
\end{aligned} \tag{45}$$

As we will see in section IV A, these contributions play a central role for the description of Zener tunneling within the vector-potential representation.

Let us now come to the first term. This, in turn, is the sum of different contributions, corresponding to the various parts of the Hamiltonian. The total Hamiltonian can be regarded as the sum of two terms, a single-particle contribution plus a many-body one:

$$\mathbf{H} = \mathbf{H}_{sp} + \mathbf{H}_{mb} = (\mathbf{H}^\circ_c + \mathbf{H}_{cl} + \mathbf{H}_p) + (\mathbf{H}_{cc} + \mathbf{H}_{cp} + \mathbf{H}_{pp}) \ . \tag{46}$$

The explicit form of the time evolution due to the single-particle Hamiltonian $\mathbf{H}_{sp}$ (non-interacting carriers plus carrier-light interaction plus free phonons) is given by:

$$\begin{aligned}
\left.\frac{d}{dt} f^e_{i_1 i_2}\right|_{sp} &= \frac{1}{i\hbar}\Bigg\{ \sum_{i_3 i_4} \left[\epsilon^e_{i_2 i_4}\delta_{i_1 i_3} - \epsilon^e_{i_3 i_1}\delta_{i_2 i_4}\right] f^e_{i_3 i_4} \\
&\qquad + \sum_{j_1} \left[U_{i_2 j_1} p^*_{j_1 i_1} - U^*_{i_1 j_1} p_{j_1 i_2}\right] \Bigg\} \\
\left.\frac{d}{dt} f^h_{j_1 j_2}\right|_{sp} &= \frac{1}{i\hbar}\Bigg\{ \sum_{j_3 j_4} \left[\epsilon^h_{j_2 j_4}\delta_{j_1 j_3} - \epsilon^h_{j_3 j_1}\delta_{j_2 j_4}\right] f^h_{j_3 j_4} \\
&\qquad + \sum_{i_1} \left[U_{i_1 j_2} p^*_{j_1 i_1} - U^*_{i_1 j_1} p_{j_2 i_1}\right] \Bigg\} \\
\left.\frac{d}{dt} p_{j_1 i_1}\right|_{sp} &= \frac{1}{i\hbar}\Bigg\{ \sum_{i_2 j_2} \left[\epsilon^h_{j_1 j_2}\delta_{i_1 i_2} + \epsilon^e_{i_1 i_2}\delta_{j_1 j_2}\right] p_{j_2 i_2} \\
&\qquad + \sum_{i_2 j_2} U_{i_2 j_2} \left[\delta_{i_1 i_2}\delta_{j_1 j_2} - f^e_{i_2 i_1}\delta_{j_1 j_2} - f^h_{j_2 j_1}\delta_{i_1 i_2}\right] \Bigg\}
\end{aligned} \tag{47}$$

with $U_{i_1 j_1} = -\mu^{eh}_{i_1 j_1} E^-(t)$.

This is a closed set of equations, which is a consequence of the single-particle nature of $\mathbf{H}_{sp}$. In addition, we stress that the structure of the two contributions entering equation (44) is very similar: one can include the contribution (45) into (47) by replacing ϵ with $\epsilon + Z$.

Let us finally discuss the contributions due to the many-body part of the Hamiltonian: carrier-carrier and carrier-phonon interactions (the phonon-phonon one is not explicitly considered here). As discussed in[64], for both interaction mechanisms one can derive a hierarchy of equations involving higher-order density matrices. In order to close such equations with respect to our set of kinetic variables, approximations are needed. The lowest-order contributions to our equations of motion are given by first-order terms in the many-body Hamiltonian: Hartree-Fock level. Since we will neglect coherent-phonon states, the only Hartree-Fock contributions will come from carrier-carrier interaction. They simply result in a renormalization

$$\Delta\epsilon^{e/h}_{l_1 l_2} = -\sum_{l_3 l_4} V^{cc}_{l_1 l_3 l_2 l_4} f^{e/h}_{l_3 l_4} \tag{48}$$

of the single-particle energy matrices $\epsilon^{e/h}$ as well as in a renormalization

$$\Delta U_{i_1 j_1} = -\sum_{i_2 j_2} V^{cc}_{i_1 j_1 j_2 i_2} p_{j_2 i_2} \tag{49}$$

of the external field U. [2] We stress that the Hartree-Fock approximation, which consists in factorizing average values of four-point operators into products of two density matrices, is independent from the quantum-mechanical picture. It is then clear that the above kinetic equations are valid in any quantum-mechanical representation.

All the contributions to the system dynamics discussed so far describe a fully coherent dynamics, i.e. no scattering processes. In order to treat incoherent phenomena, e.g. energy relaxation and dephasing, one has to go one step further in the perturbation expansion taking into account also second-order contributions (in the perturbation Hamiltonian $\mathbf{H}_{mb}$). The derivation of these higher-order contributions, discussed in[64], will not be repeated here. Again, in order to obtain a closed set of equations (with respect to our set of kinetic variables (38-39)) additional approximations are needed, namely the mean-field and Markov approximations. As for the Hartree-Fock case, the mean-field

[2] The explicit form of the renormalization terms considered in this paper accounts for the Fock contributions only, i.e. no Hartree terms. The general structure of Hartree-Fock contributions, relevant for the case of a strongly non-homogeneous system, is discussed in[64].

approximation allows to write the various higher-order density matrices as products of single-particle ones. The Markov approximation allows to eliminate the additional higher-order kinetic variables, e.g. phonon-assisted density matrices, providing a closed set of equations still local in time, i.e. no memory effects[81–85]. This last approximation is not performed in the quantum-kinetic theory discussed in[64] where, in addition to our single-particle variables, one considers two-particle[79] and phonon-assisted[84] density matrices.

While the mean-field approximation is representation-independent, this is unfortunately not the case for the Markov limit. This clearly implies that the validity of the Markov approximation is strictly related to the quantum-mechanical representation considered.

The above kinetic description, based on intra- and interband density matrices, allows us to evaluate any single-particle quantity. In particular, for the analysis of the ultrafast carrier dynamics in photoexcited semiconductors two physical quantities play a central role: the intra- and interband total (or macroscopic) polarizations:

$$P^{e/h}(t) = \sum_{ll'} M^{e/h}_{ll'} f^{e/h}_{l'l}(t) \ , \qquad P^{eh} = \sum_{ij} \mu^{eh}_{ij} p_{ji}(t) \ , \tag{50}$$

where $M^{e/h}$ and μ^{eh} denote, respectively, the intra- and interband dipole matrix elements in our ϕ-representation. The time derivative of the intraband polarization $P^{e/h}$ describes the radiation field induced by the Bloch-oscillation dynamics (which for a superlattice structure is in the TeraHertz range) while the Fourier transform of the interband (or optical) polarization P^{eh} provides the linear and non-linear optical response of the system.

III. COHERENT ULTRAFAST DYNAMICS IN BULK SEMICONDUCTORS

In this section, we will discuss the dominant role played by optically-induced phase coherence on the ultrafast generation and relaxation of photoexcited carriers in bulk semiconductors. In particular, we will compare the description based on the theoretical approach discussed above with the more conventional picture based on the Boltzmann theory.

A. Bloch model

In order to study the ultrafast carrier dynamics in bulk systems, let us consider a two-band semiconductor model. For the case of a homogeneous system, the only relevant terms of the single-particle density matrix in $\mathbf{k}$-space are the diagonal ones. This property, due to the translational symmetry of the Hamiltonian, reduces the set of kinetic variables (38-39) to the following electron and hole distribution functions (intraband density-matrix elements)

$$f^e_{\mathbf{k}} = \left\langle c^\dagger_{\mathbf{k}} c_{\mathbf{k}} \right\rangle \ , \qquad f^h_{-\mathbf{k}} = \left\langle d^\dagger_{-\mathbf{k}} d_{-\mathbf{k}} \right\rangle \tag{51}$$

together with the corresponding polarizations (interband density-matrix elements) [3]

$$p_{\mathbf{k}} = \left\langle d_{-\mathbf{k}} c_{\mathbf{k}} \right\rangle \ . \tag{52}$$

The explicit form of the kinetic equations (44) within the above two-band picture is given by

$$\frac{d}{dt} f^e_{\mathbf{k}} = g_{\mathbf{k}}(t) - \sum_{\mathbf{k}'} \left[W^e_{\mathbf{k}'\mathbf{k}} f^e_{\mathbf{k}} \left(1 - f^e_{\mathbf{k}'}\right) - W^e_{\mathbf{k}\mathbf{k}'} f^e_{\mathbf{k}'} \left(1 - f^e_{\mathbf{k}}\right) \right]$$

$$\frac{d}{dt} f^h_{\mathbf{k}} = g_{-\mathbf{k}}(t) - \sum_{\mathbf{k}'} \left[W^h_{\mathbf{k}'\mathbf{k}} f^h_{\mathbf{k}} \left(1 - f^h_{\mathbf{k}'}\right) - W^h_{\mathbf{k}\mathbf{k}'} f^h_{\mathbf{k}'} \left(1 - f^h_{\mathbf{k}}\right) \right]$$

[3] Here, the standard electron-hole picture introduced in section II A has been applied to our plane-wave states. In particular, due to the charge-conjugation symmetry, the hole states are still labeled in terms of the corresponding valence-electron states, i.e. $\mathbf{k}^h \equiv -\mathbf{k}^e$.

$$\frac{d}{dt}p_{\mathbf{k}} = \frac{1}{i\hbar}\left[\left(\epsilon^e_{\mathbf{k}} + \epsilon^h_{-\mathbf{k}}\right)p_{\mathbf{k}} + U_{\mathbf{k}}\left(1 - f^e_{\mathbf{k}} - f^h_{-\mathbf{k}}\right)\right] - \sum_{\mathbf{k}'}\left[W^p_{\mathbf{k}'\mathbf{k}}p_{\mathbf{k}} - W^p_{\mathbf{k}\mathbf{k}'}p_{\mathbf{k}'}\right] \ , \tag{53}$$

with the generation rate

$$g_{\mathbf{k}} = \frac{1}{i\hbar}\left[U_{\mathbf{k}}p^*_{\mathbf{k}} - U^*_{\mathbf{k}}p_{\mathbf{k}}\right] \ . \tag{54}$$

Here, the incoherent contributions are treated within the usual Markov limit as described in[64,67,70]. Within such approximation scheme, the incoherent contributions to the polarization dynamics exhibit the same structure as for the distribution functions in terms of the following in- and out-scattering rates

$$W^p_{\mathbf{k}'\mathbf{k}} = \frac{1}{2}\sum_{\nu=e,h}\left[W^\nu_{\mathbf{k}'\mathbf{k}}\left(1 - f^\nu_{\mathbf{k}'}\right) + W^\nu_{\mathbf{k}'\mathbf{k}}f^\nu_{\mathbf{k}'}\right] \ , \tag{55}$$

where $W^{e/h}_{\mathbf{k}'\mathbf{k}}$ are the usual scattering rates of the semiclassical Boltzmann theory. This Boltzmann-like structure of the scattering term in the polarization equation is the starting point of the generalized Monte Carlo method discussed in section I[66–70].

The above kinetic equations are known as *semiconductor Bloch equations* (SBE)[4]. As we can see, here the carrier photogeneration is a two-step process: The external field U induces a coherent polarization p which, in turn, generates electron-hole pairs via its coupling with the field according to equation (54). The generation rate is thus determined by the interband polarization $p_{\mathbf{k}}$ which, in turn, is influenced by the various density-dependent scattering mechanisms, e.g. carrier-carrier processes. Therefore, in contrast to the semiclassical case discussed below, the generation rate within the SBE model is clearly density dependent.

B. Boltzmann model

The conventional Boltzmann model is obtained from the above SBE by performing an adiabatic elimination of the interband polarization $p_{\mathbf{k}}$, i.e. by inserting a formal solution of the polarization equation into the generation rate (54) and then performing a Markov limit with respect to the electron and hole distribution functions[67,70]. This corresponds to assuming that the carrier distributions are slowly-varying functions on the time-scale of the laser photoexcitation, i.e. the carrier generation and relaxation are treated as independent processes. Within such approximation scheme, except for phase-space-filling effects, the generation rate entering the semiclassical Boltzmann equations (BE) for electrons and holes is fully determined by the temporal and spectral characteristics of the laser pulse. Contrary to the SBE case, all effects related to the optically induced phase coherence —and to its temporal decay— are neglected.

C. Coherent carrier photogeneration

In order to compare the different models of carrier dynamics in photoexcited semiconductors, let us review some simulated experiments[74] based on the generalized Monte Carlo solution of the SBE[66–70] discussed in section I. The corresponding BE has been solved, for comparison, by a standard ensemble Monte Carlo (EMC) simulation[27,29]. Both BE and SBE have been solved numerically for the case of GaAs bulk excited by a 150 fs laser pulse.

In figure 1 the generation rate at different times as obtained from the SBE is plotted as a function of the carrier wave vector for three different densities. At the lowest density the behavior is essentially the same as in the case without carrier-carrier scattering: Energy-time uncertainty leads to an initially very

[4]In the absence of Coulomb correlation and scattering, the SBE in (53) reduce to the optical Bloch equations introduced in section I C, i.e. they describe a collection of independent (non-interacting) two-level systems.

broad generation rate; with increasing time the line narrows and, in the tails, exhibits negative parts due to a stimulated recombination of carriers initially generated off-resonance[67,70]. After the pulse, the distribution function of the generated carriers is in good agreement with the BE result. Scattering processes destroy the coherence between electrons and holes which is necessary for the stimulated recombination processes. As a consequence, with increasing density the negative tails are strongly reduced and the generation remains broad for all times resulting in a much broader carrier distribution than in the BE case.

D. Comparison with experiments

Hot carrier luminescence has proven to be a powerful technique to study the ultrafast dynamics of photoexcited carriers in semiconductors[18]. In band-to-acceptor (BA) luminescence experiments[19,21,86,87], due to their high sensitivity, carrier densities as low as several 10^{13} cm^{-3} have been reached. Thus, the transition between a dynamics dominated by carrier-phonon scattering to a dynamics dominated by carrier-carrier scattering (with its consequences for the generation process discussed above) is experimentally accessible.

In the BA luminescence experiment reviewed here[73–75], a 3 μm thick GaAs layer doped with Be acceptors of a concentration of 3×10^{16} cm^{-3} is excited at a photon energy of 1.73 eV by transform limited 150 fs pulses from a mode-locked Ti:sapphire laser. Time-integrated luminescence spectra are recorded[73]. The right column of figure 2 shows measured BA luminescence spectra for three different values of the carrier density. At low density we observe an initial peak of the generated carriers (marked bold) and pronounced replicas due to the emission of an integer number of optical phonons. With increasing density the peaks become broader and at the highest density only a slight structure related to the phonons is still visible.

These measured spectra are compared with corresponding simulated experiments based on the BE and SBE models[74] (left and middle column in figure 2). We find several pronounced differences between the two models. In the semiclassical model the unrelaxed peak is clearly visible up to the highest density in contrast to the coherent model, where, in agreement with the experiment, this peak is strongly broadened. At the higher densities the semiclassical spectra exhibit an increase in the broadening of subsequent replicas which is not present in the Bloch-model calculations as well as in the experimental results.

To illustrate this difference quantitatively, in figure 3 we have plotted the full width at half maximum (FWHM) of the three highest peaks in the spectra. From the semiclassical model we obtain a strong increase in the density dependence of subsequent peaks. This behavior can be easily understood: Due to the emission time of an optical phonon of about 150 fs, the carriers populate subsequent replicas at increasing times and, therefore, the efficiency of carrier-carrier scattering processes in broadening the peaks increases. However, the measured spectra exhibit a different behavior which is quantitatively reproduced by the SBE model: Already the unrelaxed peak exhibits a strong increase with increasing density and the density dependence of all replicas is approximately the same. The reason is that the broadening of the generation process as discussed above obviously dominates over the broadening due to subsequent scattering processes. As discussed in[75], this is due to the fact that the generation process is strongly influenced by the decay of the interband polarization which, in turn, is due to electron plus hole scattering, while the broadening of the electron distribution during the relaxation process is due to electron scattering only. [5]

The above theoretical and experimental analysis constitutes a clear demonstration of the importance of dephasing processes for the analysis of luminescence spectra. The density dependence of the spectra in the interesting transition region between carrier-phonon and carrier-carrier dominated dynamics can only be explained by a coherent modeling of the carrier generation including the dynamics of the interband polarization. The main mechanism determining the width of the peaks is the broadening of the generation rate. It can be shown that for band-to-acceptor spectra the broadening of the recombination process, neglected in the present model, plays a minor role[74]. However, for band-to-band spectra also this phenomenon should be taken into account. For the case discussed above the background due to band-to-band luminescence has been found to be of negligible importance[75].

---

[5] For the case of bulk GaAs considered here, due to the different electron and heavy-hole effective masses, the hole-hole scattering is about 5 times larger than the electron-electron one.

IV. BLOCH OSCILLATIONS AND WANNIER-STARK LOCALIZATION IN SUPERLATTICES

Ever since the initial applications of quantum mechanics to the dynamics of electrons in solids, the analysis of Bloch electrons moving in a homogeneous electric field has been of central importance. By employing semiclassical arguments, in 1928 Bloch[88] demonstrated that, a wave packet given by a superposition of single-band states peaked about some quasimomentum, $\hbar\mathbf{k}$, moves with a group velocity given by the gradient of the energy-band function with respect to the quasimomentum and that the rate of change of the quasimomentum is proportional to the applied field $\mathbf{F}$. This is often referred to as the "acceleration theorem":

$$\hbar\dot{\mathbf{k}} = e\mathbf{F} \ . \tag{56}$$

Thus, in the absence of interband tunneling and scattering processes, the quasimomentum of a Bloch electron in a homogeneous and static electric field will be uniformly accelerated into the next Brillouin zone in a repeated-zone scheme (or equivalently undergoes an Umklapp process back in to the first zone). The corresponding motion of the Bloch electron through the periodic energy-band structure, shown in figure 4, is called "Bloch oscillation"; It is characterized by an oscillation period $\tau_B = h/eFd$, where d denotes the lattice periodicity in the field direction.

There are two mechanisms impeding a fully periodic motion: interband tunneling and scattering processes. Interband tunneling is an intricate problem and still at the center of a continuing debate. Early calculations of the tunneling probability into other bands in which the electric field is represented by a time-independent scalar potential were made by Zener[89] using a Wentzel-Kramers-Brillouin generalization of Bloch functions, by Houston[90] using accelerated Bloch states (Houston states), and subsequently by Kane[91] and Argyres[92] who employed the crystal-momentum representation. Their calculations lead to the conclusion that the tunneling rate per Bloch period is much less than unity for electric fields up to 10^6V/cm for typical band parameters corresponding to elemental or compound semiconductors.

Despite the apparent agreement among these calculations, the validity of employing the crystal-momentum representation or Houston functions to describe electrons moving in a non-periodic (crystal plus external field) potential has been disputed. The starting point of the controversy was the original paper by Wannier[93]. He pointed out that, due to the translational symmetry of the crystal potential, if $\phi(\mathbf{r})$ is an eigenfunction of the scalar-potential Hamiltonian (corresponding to the perfect crystal plus the external field) with eigenvalue ϵ, then any $\phi(\mathbf{r}+n\mathbf{d})$ is also an eigenfunction with eigenvalue $\epsilon+n\Delta\epsilon$, where $\Delta\epsilon = eFd$ is the so-called Wannier-Stark splitting ($\mathbf{d}$ being the primitive lattice vector along the field direction). He concluded that the translational symmetry of the crystal gives rise to a discrete energy spectrum, the so-called Wannier-Stark ladder. The states corresponding to these equidistantly spaced levels are localized states, as schematically shown in figure 5 for the case of a semiconductor superlattice.

The existence of such energy quantization was disputed by Zak[94], who pointed out that for the case of an infinite crystal the scalar potential $-\mathbf{F}\cdot\mathbf{r}$ is not bounded, which implies a continuous energy spectrum. Thus, the main point of the controversy was related to the existence (or absence) of Wannier-Stark ladders. More precisely, the point was to decide if interband tunneling (neglected in the original calculation by Wannier[93]) is so strong to destroy the Wannier-Stark energy quantization (and the corresponding Bloch oscillations) or not.

It is only during the last decade that this controversy came to an end. From a theoretical point of view, most of the formal problems related to the non-periodic nature of the scalar potential (superimposed to the periodic crystal potential) were finally removed by using a vector-potential representation of the applied field[95,96]. Within such vector-potential picture, upper boundaries for the interband tunneling probability have been established at a rigorous level, which show that an electron may execute a number of Bloch oscillations before tunneling out of the band[96,97], in qualitatively good agreement with the earlier predictions of Zener and Kane[89,91].

The second mechanism impeding a fully periodic motion is scattering by phonons, impurities, etc. (see figure 4). This results in lifetimes shorter than the Bloch period τ_B for all reasonable values of the electric field, so that Bloch oscillations should not be observable in conventional solids.

In superlattices, however, the situation is much more favourable because of the smaller Bloch period τ_B resulting from the small width of the mini-Brillouin zone in the field direction[98].

Indeed, the existence of Wannier-Stark ladders as well as Bloch oscillations in superlattices has been confirmed by a number of recent experiments[1]. The photoluminescence and photocurrent measurements of the biased GaAs/GaAlAs superlattices performed by Mendez and coworkers[99], together with

the electroluminescence experiments by Voisin and coworkers[100], provided the earliest evidence of the field-induced Wannier-Stark ladders in superlattices. A few years later, Feldmann and coworkers[101] were able to measure Bloch oscillations in the time domain through a four-wave-mixing experiment originally suggested by von Plessen and Thomas[102]. A detailed analysis of the Bloch oscillations in the four-wave-mixing signal (which reflects the interband dynamics) has been also performed by Leo and coworkers[103,104].

In addition to the above interband-polarization analysis, Bloch oscillations have been also detected by monitoring the intraband polarization which, in turn, is reflected by anisotropic changes in the refractive index[1]. Measurements based on transmittive electrooptic sampling (TEOS) have been performed by Dekorsy and coworkers[105,106]. Finally Bloch oscillations were recently measured through a direct detection of the TeraHertz (THz) radiation in semiconductor superlattices[44,107].

A. Two equivalent pictures

Let us now apply the theoretical approach presented in section II to the case of a semiconductor superlattice in the presence of an uniform (space-independent) electric field. The non-interacting carriers within the superlattice crystal will then be described by the Hamiltonian $\mathbf{H}_c^\circ$ in equation (23), where now the electrodynamic potentials $\mathbf{A}_2$ and φ_2 (in the following simply denoted with $\mathbf{A}$ and φ) correspond to a homogeneous electric field $\mathbf{E}_2(\mathbf{r},t)=\mathbf{F}(t)$.

As pointed out in section II A, the natural quantum-mechanical representation is given by the eigenstates of this Hamiltonian:

$$\left[\frac{\left(-i\hbar\nabla_{\mathbf{r}}-\frac{e}{c}\mathbf{A}(\mathbf{r},t)\right)^2}{2m_\circ}+e\varphi(\mathbf{r},t)+V^l(\mathbf{r})\right]\phi_n(\mathbf{r})=\epsilon_n\phi_n(\mathbf{r})\ . \tag{57}$$

However, due to the gauge freedom discussed in section II A, there is an infinite number of possible combinations of $\mathbf{A}$ and φ —and therefore of possible Hamiltonians— which describe the same homogeneous electric field $\mathbf{F}(t)$. In particular, one can identify two independent choices: the vector-potential gauge

$$\mathbf{A}(\mathbf{r},t)=-c\int_{t_\circ}^{t}\mathbf{F}(t')dt'\ ,\qquad \varphi(\mathbf{r},t)=0 \tag{58}$$

and the scalar-potential gauge

$$\mathbf{A}(\mathbf{r},t)=0\ ,\qquad \varphi(\mathbf{r},t)=-\mathbf{F}(t)\cdot\mathbf{r} \tag{59}$$

As shown in[108], the two independent choices correspond, respectively, to the well known Bloch-oscillation and Wannier-Stark pictures. They simply reflect two equivalent quantum-mechanical representations and, therefore, any physical phenomenon can be described in both pictures.

More specifically, within the vector-potential picture (58), the eigenfunctions ϕ_n in (57) are the so-called accelerated Bloch states (or Houston states)[90,95,96]. As discussed in[108], such time dependent representation constitutes the natural basis for the description of Bloch oscillations, i.e. it provides a rigorous quantum-mechanical derivation of the acceleration theorem (56), thus showing that this is not a simple semiclassical result. [6] Within such representation, Bloch oscillations are fully described by the diagonal terms of the intraband density matrix (38) (semiclassical distribution functions). Therefore, non-diagonal elements, describing phase-coherence between different Bloch states, do not contribute to the intraminiband dynamics. However, they are of crucial importance for the description of interminiband dynamics, i.e. field-induced Zener tunneling, which in this Bloch-state representation originates from the time variation of our basis states (see equation (45)).

On the contrary, within the scalar-potential picture (59), the eigenfunctions ϕ_n in (57) are the well-known Wannier-Stark states[93]. Contrary to the previous Bloch picture, within such representation the intraminiband Bloch dynamics originates from a quantum interference between different Wannier-Stark states, thus involving non-diagonal elements of the intraband density matrix (38).

---

[6] The acceleration theorem (56) and the corresponding Bloch-oscillation dynamics are usually regarded as a semiclassical result compared to the Wannier-Stark picture. On the contrary, they correspond to two different fully quantum-mechanical pictures.

B. Some simulated experiments

In this section, we will review recent simulated experiments of the ultrafast carrier dynamics in semiconductor superlattices[109–114]. They are based on a generalized Monte Carlo solution[66–70] of the set of kinetic equations (so-called semiconductor Bloch equations) derived in section II B. In this case, the Bloch representation discussed in section IV A has been employed limiting the set of interband density-matrix elements in (39) to the diagonal ones, i.e. $i = j$. In addition, incoherent scattering processes have been treated within the usual Markov limit as discussed in[64,67,70]. Within such approximation scheme, the explicit form of the kinetic equations (44) coincides with the SBE (17) (obtained for the bulk case)[108], provided we replace the wavevector $\mathbf{k}$ with $\mathbf{k}\nu$, ν being the superlattice miniband index.

In the simulated experiments reviewed here the following superlattice model has been employed: The energy dispersion and the corresponding wavefunctions along the growth direction ($k_\parallel$) are computed within the well known Kronig-Penney model[98], while for the in-plane direction ($k_\perp$) an effective-mass model has been used. Starting from these three-dimensional wavefunctions $\phi^\circ_{\mathbf{k}\nu}$, the various carrier-carrier as well as carrier-phonon matrix elements are numerically computed (see equations (35) and (37)). They are, in general, functions of the various miniband indices and depend separately on $k_\parallel$ and $k_\perp$, thus fully reflecting the anisotropic nature of the superlattice structure.

Only coupling to GaAs bulk phonons has been considered. This, of course, is a simplifying approximation which neglects any superlattice effect on the phonon dispersion, such as confinement of optical modes in the wells and in the barriers, and the presence of interface modes[115,116]. However, while these modifications have important consequences for phonon spectroscopies (like Raman scattering), they are far less decisive for transport phenomena. [7]

We will start discussing the scattering-induced damping of Bloch oscillations. In particular, we will show that in the low-density limit this damping is mainly determined by optical-phonon scattering[109,110] while at high densities the main mechanism responsible for the suppression of Bloch oscillations is found to be carrier-carrier scattering[114].

This Bloch-oscillation analysis in the time domain is also confirmed by its counterpart in the frequency domain. As pointed out in section IV A, the presence of Bloch oscillations, due to a negligible scattering dynamics, should correspond to Wannier-Stark energy quantization. This is confirmed by the simulated optical-absorption spectra, which clearly show the presence of the field-induced Wannier-Stark ladders[113].

1. Bloch-oscillation analysis

All the simulated experiments presented in this section refer to the superlattice structure considered in Ref.[111]: 111 Å GaAs wells and 17 Å $Al_{0.3}Ga_{0.7}As$ barriers. For such a structure there has been experimental evidence for a THz-emission from Bloch oscillations[107].

In the first set of simulated experiments an initial distribution of photoexcited carriers (electron-hole pairs) is generated by a 100 fs Gaussian laser pulse in resonance with the first-miniband exciton ($\hbar\omega_L \approx$ 1540 meV). The strength of the applied electric field is assumed to be 4 kV/cm, which corresponds to a Bloch period $\tau_B = h/eFd$ of about 800 fs.

In the low-density limit (corresponding to a weak laser excitation), incoherent scattering processes do not alter the Bloch-oscillation dynamics. This is due to the following reasons: In agreement with recent experimental[107,117] and theoretical[109–111] investigations, for superlattices characterized by a miniband width smaller than the LO-phonon energy —as for the structure considered here— and for laser excitations close to the band gap, at low temperature carrier-phonon scattering is not permitted. Moreover, in this low-density regime carrier-carrier scattering plays no role: Due to the quasi-elastic nature of Coulomb collisions, in the low-density limit the majority of the scattering processes is characterized by a very small momentum transfer; As a consequence, the momentum relaxation along the growth direction is negligible. As a result, on this picosecond time-scale the carrier system exhibits a coherent Bloch-oscillation dynamics, i.e. a negligible scattering-induced dephasing. This can be clearly seen

[7] Indeed, by now it is well known[116] that the total scattering rates are sufficiently well reproduced if the phonon spectrum is assumed to be bulk-like.

from the time evolution of the carrier distribution as a function of $k_\parallel$ (i.e. averaged over $k_\perp$) shown in figure 6. During the laser photoexcitation ($t = 0$) the carriers are generated around $k_\parallel = 0$, where the transitions are close to resonance with the laser excitation. According to the acceleration theorem (56), the electrons are then shifted in **k**-space. When the carriers reach the border of the first Brillouin zone they are Bragg reflected. After about 800 fs, corresponding to the Bloch period τ_B, the carriers have completed one oscillation in **k**-space. As expected, the carriers execute Bloch oscillations without loosing the synchronism of their motion by scattering. This is again shown in figure 6, where we have plotted: (b) the mean kinetic energy, (c) the current, and (d) its time derivative which is proportional to the emitted far field, i.e. the THz-radiation. (It can be shown that, by neglecting Zener tunneling, the intraband polarization $P^{e/h}$ in equation (50) is proportional to the current.) All these three quantities exhibit oscillations characterized by the same Bloch period τ_B. Due to the finite width of the carrier distribution in **k**-space (see figure 6(a)), the amplitude of the oscillations of the kinetic energy is somewhat smaller than the miniband width. Since for this excitation condition the scattering-induced dephasing is negligible, the oscillations of the current are symmetric around zero, which implies that the time average of the current is equal to zero, i.e. no dissipation.

As already pointed out, this ideal Bloch-oscillation regime is typical of a laser excitation close to gap in the low-density limit. Let us now discuss, still at low densities, the case of a laser photoexcitation high in the band. Figure 7(a) shows the THz-signal as obtained from a set of simulated experiments corresponding to different laser excitations[111]. The different traces correspond to the emitted THz-signal for increasing excitation energies. We clearly notice the presence of Bloch oscillations in all cases. However, the oscillation amplitude and decay (effective damping) is excitation-dependent.

For the case of a laser excitation resonant with the first-miniband exciton considered above (see figure 6), we have a strong THz-signal. The amplitude of the signal decreases when the excitation energy is increased. Additionally, there are also some small changes in the phase of the oscillations, which are induced by the electron-LO phonon scattering.

When the laser energy comes into resonance with the transitions between the second electron and hole minibands ($\hbar\omega_L \approx 1625$ meV), the amplitude of the THz-signal increases again. The corresponding THz-transients show an initial part, which is strongly damped and some oscillations for longer times that are much less damped. For a better understanding of these results, we show in figure 7(b) the individual THz-signals, originating from the two electron and two heavy-hole minibands for the excitation with $\hbar\omega = 1640$ meV. The Bloch oscillations performed by the electrons within the second miniband are strongly damped due to intra- and interminiband LO-phonon scattering processes[109,111]. Since the width of this second miniband (45 meV) is somewhat larger than the LO-phonon energy, also intraminiband scattering is possible, whenever the electrons are accelerated into the high-energy region of the miniband. The THz-signal originating from electrons within the first miniband shows an oscillatory behavior with a small amplitude and a phase which is determined by the time the electrons need to relax down to the bottom of the band.

At the same time, the holes in both minibands exhibit undamped Bloch oscillations, since the minibands are so close in energy that for these excitation conditions no LO-phonon emission can occur. The analysis shows that at early times the THz-signal is mainly determined by the electrons within the second miniband. At later times the observed signal is due to heavy holes and electrons within the first miniband.

The above theoretical analysis closely resembles experimental observations obtained for a superlattice structure very similar to the one modelled here[107]. In these experiments, evidence for THz-emission from Bloch oscillations has been reported. For some excitation conditions these oscillations are associated with resonant excitation of the second miniband. The general behavior of the magnitude of the signals, the oscillations and the damping are close to the results shown in figure 7.

Finally, in order to study the density dependence of the Bloch-oscillation damping, let us go back to the case of laser excitations close to gap. Figure 8(a) shows the total (electrons plus holes) THz-radiation as a function of time for three different carrier densities. With increasing carrier density, carrier-carrier scattering becomes more and more important: Due to Coulomb screening, the momentum transfer in a carrier-carrier scattering increases (its typical value being comparable with the screening wavevector). This can be seen in figure 8(a), where for increasing carrier densities we realize an increasing damping of the THz-signal. However, also for the highest carrier density considered here we deal with a damping time of the order of 700 fs, which is much larger than the typical dephasing time, i.e. the decay time of the interband polarization, associated with carrier-carrier scattering. The dephasing time is typically investigated by means of four-wave-mixing (FWM) measurements and such multi-pulse experiments can be simulated as well[71,72]. From a theoretical point of view, a qualitative estimate of the dephasing time is given by the decay time of the "incoherently summed" polarization (ISP)[67]. Figure 8(b) shows

such ISP as a function of time for the same three carrier densities of figure 8(a). As expected, the decay times are always much smaller than the corresponding damping times of the THz-signals (note the different time-scale in figures 8(a) and (b)). This difference, discussed in more detail in[114,108], can be understood as follows: The fast decay times of figure 8(b) reflect the interband dephasing, i.e. the sum of the electron and hole scattering rates. In particular, for the Coulomb interaction this means the sum of electron-electron, electron-hole, and hole-hole scattering. As for the case of bulk GaAs discussed in section III, this last contribution is known to dominate and determines the dephasing time-scale. On the other hand, the total THz-radiation in figure 8(a) is the sum of the electron and hole contributions. However, due to the small value of the hole miniband width compared to the electron one, the electron contribution will dominate. This means that the THz damping in figure 8(a) mainly reflects the damping of the electron contribution. This decay, in turn, reflects the intraband dephasing of electrons which is due to electron-electron and electron-hole scattering only, i.e. no hole-hole contributions.

From the above analysis we can conclude that the decay time of the THz-radiation due to carrier-carrier scattering differs considerably from the corresponding dephasing times obtained from a FWM experiment: The first one is a measurement of the intraband dephasing while the second one reflects the interband dephasing. [8]

2. Optical-absorption analysis

Let us now discuss the frequency-domain counterpart of the Bloch-oscillation picture considered so far. Similar to what happens in the time domain, for sufficiently high electric fields, i.e. when the Bloch period $\tau_B = h/eFd$ becomes smaller than the dephasing time, the optical spectra of the superlattice are expected to exhibit the frequency-domain counterpart of the Bloch oscillations, i.e. the Wannier-Stark energy quantization discussed in section IV A. In the absence of Coulomb interaction, the Wannier-Stark ladder absorption increases as a function of the photon energy in a step-like fashion. These steps are equidistantly spaced. Their spacing, named Wannier-Stark splitting, is proportional to the applied electric field.

The simulated linear-absorption spectra corresponding to a superlattice structure with 95 Å GaAs wells and 15 Å $Al_{0.3}Ga_{0.7}As$ barriers are shown in figure 9[113]. As we can see, the Coulomb interaction gives rise to excitonic peaks in the absorption spectra and introduces couplings between these Wannier-Stark states. Such exciton peaks, which are no longer equidistantly spaced, are often referred to as excitonic Wannier-Stark ladders[118] of the superlattice.

Since for the superlattice structure considered in this simulated experiment[109,113] the combined miniband width is larger than the typical two- and three-dimensional exciton binding energies, it is possible to investigate the quasi-three dimensional absorption behavior of the delocalized miniband states as well as localization effects induced by the electric field.

For the free-field case, the electron and hole states are completely delocalized in our three-dimensional **k**-space. The perturbation induced by the application of a low field (here $\approx$ 5 kV/cm), couples the states along the field direction and in the spectra the Franz-Keldysh effect, well known from bulk materials[8], appears: one clearly notices oscillations which increase in amplitude with the field and shift with $F^{2/3}$ from the $n = 0$ and $n = 1$ levels toward the center of the combined miniband.

For increasing field the potential drop over the distance of a few quantum wells eventually exceeds the miniband width and the electronic states become more and more localized. Despite the field-induced energy difference $neFd$, the superlattice potential is equal for quantum wells separated by nd. Therefore, the spectra decouple into a series of peaks corresponding to the excitonic ground states of the individual electron-hole Wannier-Stark levels. Each Wannier-Stark transition contributes to the absorption with a pronounced $1-s$ exciton peak, plus higher bound exciton and continuum states. The oscillator strength of a transition n is proportional to the overlap between electron and hole wavefunctions centered at quantum wells n' and $n + n'$, respectively. The analysis shows that this oscillator strength is almost exclusively determined by the amplitude of the electron wavefunction in quantum well $n' + n$ since

[8] We stress that this difference between intraband and interband dephasing in superlattices is the same discussed in section III for the case of bulk semiconductors, where the broadening of the photoexcited carrier distribution is mainly determined by the decay of the interband polarization (interband dephasing) while the subsequent energy broadening of the electron distribution is due to electron scattering only (intraband dephasing) (see figure 2).

for fields in the Wannier-Stark regime the hole wavefunctions are almost completely localized over one quantum well due to their high effective mass (see figure 5). Thus, the oscillator strengths of transitions to higher $|n|$ become smaller with increasing $|n|$ and field.

At high fields (here $>\approx 8$ kV/cm) the separation between the peaks is almost equal to $neFd$. For example, the peak of the $n = 0$ transition which is shifted by the Wannier-Stark exciton binding energy with respect to the center of the combined miniband, demonstrates that the increasing localization also increases the exciton binding energy. This increased excitonic binding reflects the gradual transition from a three- to a two-dimensional behavior, discussed in detail in[111].

For intermediate fields there is an interplay between the Wannier-Stark and the Franz-Keldysh effect. Coming from high fields, first the Wannier-Stark peaks are modulated by the Franz-Keldysh oscillations. However, as soon as the separation eFd between neighboring peaks becomes smaller than their spectral widths, the peaks can no longer be resolved individually so that only the Franz-Keldysh structure remains.

V. COULOMB-CORRELATION EFFECTS IN SEMICONDUCTOR QUANTUM WIRES

The importance of Coulomb-correlation effects in optical spectra of semiconductors and their dependence on dimensionality has now been long recognized[119]. More recently, increasing interest has been devoted to one-dimensional (1D) systems[120], prompted by promising advances in quantum-wire fabrication and application, e.g. quantum-wire lasers. The main goal is to achieve structures with improved optical efficiency as compared to two-dimensional (2D) and three-dimensional (3D) ones. A common argument in favour of this effort is based on the well known van Hove divergence in the 1D joint density-of-states (DOS), which is expected to give rise to very sharp peaks in the optical spectra of 1D structures. Such prediction is however based on free-carrier properties of ideal 1D systems and it ignores Coulomb-correlation effects.

Early theoretical investigations by Ogawa and coworkers[121,122], based on a 1D single-subband model of the wires, showed that the inverse-square-root singularity in the 1D DOS at the band edge is smoothed when excitonic effects are taken into account.

In this section, we will review recent theoretical results[123–125] based on a full 3D description of realistic quantum-wire structures made available by the present technology, such as structures obtained by epitaxial growth on non-planar substrates (V-shaped wires)[126] or by cleaved-edge quantum well overgrowth (T-shaped wires)[127]. On the one hand, this approach allows an accurate determination of 1D-exciton binding energies; on the other hand, it allows us to investigate also the non linear (gain) regime. In both cases, one finds a strong suppression of the 1D band-edge singularity, in agreement with previous results based on simplified 1D models[121,122].

This theoretical approach[123,124] is based on the general kinetic theory presented in section II, which allows a full 3D description of Coulomb interaction within a multiminiband scheme. In particular, we focus on the quasi-equilibrium regime where the solution of the coupled kinetic equations (44) simply reduces to the solution of the interband-polarization equation. This is performed by direct numerical evaluation of the polarization eigenvalues and eigenvectors[124], which fully determine the absorption spectrum as well as the exciton wavefunctions. The main ingredients entering this calculation are the single-particle energies and wavefunctions, obtained numerically for the 2D confinement potential deduced, e.g., from TEM as in[126].

The above theoretical scheme has been applied to realistic V- and T-shaped wire structures. In particular, here we show results for the GaAs/AlGaAs V-wire structure of Ref.[126], whose cross-section is shown in figure 10.

A. Linear response: excitonic-absorption regime

Let us start considering the optical response of the system in the low-density limit. In figure 11 we show the linear-absorption spectra obtained when taking into account the lowest wire transition only. Results of our Coulomb-correlated (CC) approach are compared to those of the free-carrier (FC) model . As we can see, electron-hole correlation introduces two important effects: First, the excitonic peak arises below the onset of the continuum, with a binding energy of about 12 meV, in excellent agreement with recent experiments[126]. Second, one finds a strong suppression of the 1D DOS singularity. A detailed analysis of the physical origin of such suppression[123,124] has shown that the quantity which is mainly modified by CC is the oscillator strength (OS). In figure 12(a) the ratio between the CC and FC OS is

plotted as a function of excess energy (solid line). This ratio is always less than one and goes to zero at the band edge, and reflects a sort of hole in the electron-hole correlation function $g(z)$ as shown in figure 12(b). Such vanishing behaviour is found to dominate the 1D DOS singularity and, as a result, the absorption spectrum exhibits a regular behaviour at the band edge (solid line in figure 11).

The above analysis shows that also for realistic quantum-wire structures electron-hole correlation leads to a strong suppression of the 1D band-edge singularity in the linear-absorption spectrum, contrary to the 2D and 3D cases.

B. Non-linear response: gain regime

Most of the potential quantum-wire applications, i.e. 1D lasers and modulators, operate in strongly non-linear-response regimes[120]. In such conditions, the above linear-response analysis has to be generalized taking into account additional factors as: (i) screening effects, (ii) band renormalization, (iii) space-phase filling.

Figure 13 reports quantitative results for non-linear absorption spectra of realistic V-shaped wire structures at different carrier densities at room temperature. As a reference we also show the results obtained by including the lowest subband only [figure 13(a)]. In the low-density limit (case A: $n = 10^4$ cm^{-1}) we clearly recognize the exciton peak. With increasing carrier density, the strength of the excitonic absorption decreases due to phase-space filling and screening of the attractive electron-hole interaction, and moreover the band renormalization leads to a red-shift of the continuum. At a density of $4 * 10^6$ cm^{-1} (case D) the spectrum already exhibits a negative region corresponding to stimulated emission, i.e. gain regime. As desired, the well pronounced gain spectrum extends over a limited energy region (smaller than the thermal energy); However, its shape differs considerably from the ideal FC one (curve marked with diamonds in the same figure). In particular, the band-edge singularity in the ideal FC gain spectrum is clearly smeared out by electron-hole correlation. The overall effect is a broader and less pronounced gain region.

Finally, figure 13(b) shows the non-linear spectra corresponding to the realistic case of a 12-subband V-shaped wire. In comparison with the single-subband case [figure 13(a)], the multisubband nature is found to play an important role in modifying the typical shape of the gain spectra, which for both CC and FC models result to extend over a range much larger than that of the single-subband case for the present wire geometry. In addition, the Coulomb-induced suppression of the single-subband singularities, here also due to intersubband-coupling effects, tends to reduce the residual structures in the gain profile. Therefore, even in the ideal case of a quantum wire with negligible disorder and scattering-induced broadening, our analysis indicates that, for the typical structure considered, the shape of the absorption spectra over the whole density range differs considerably from the sharp FC spectrum of figure 11.

This tells us that, in order to obtain sharp gain profiles, one of the basic steps in quantum-wire technology is to produce structures with increased subband splitting. However, the disorder-induced inhomogeneous broadening, not considered here, is known to increase significantly the spectral broadening and this effect is expected to increase with increasing subband splitting. Therefore, extremely-high-quality structures (e.g. single-monolayer control) seem to be the only possible candidates for successful quantum-wire applications.

VI. SUMMARY AND CONCLUSIONS

A review of coherent phenomena in optically-excited semiconductors has been presented. Our analysis has allowed the identification of two classes of phenomena: *optically-induced* and *Coulomb-induced* coherent phenomena. We have shown that both classes can be described in terms of a unique theoretical framework based on the density-matrix formalism. Due to its generality, such quantum-kinetic approach allows a realistic description of coherent as well as incoherent, i.e. phase-breaking, processes, thus providing quantitative information on the coupled —coherent vs. incoherent— carrier dynamics in photoexcited semiconductors.

The primary goal of the paper was to discuss the concept of quantum-mechanical phase coherence as well as its relevance and implications on semiconductor physics and technology. In particular, we have analyzed the dominant role played by optically induced phase coherence on the process of ultrafast carrier photogeneration. We have then discussed typical field-induced coherent phenomena in semiconductor superlattices, e.g. Bloch oscillations and the corresponding THz radiation, as well as

their dephasing dynamics. Finally, we have analyzed the dominant role played by Coulomb correlation on the linear and non-linear optical spectra of realistic quantum-wire structures, namely the Coulomb-induced suppression of ideal 1D-band-edge singularities.

Our analysis shows that the conventional separation between coherent and incoherent regimes is no longer valid for most of the recent ultrafast optical experiments in semiconductors. The reason is that on such extremely short time-scales the carrier dynamics is the result of a strong interplay between coherence and relaxation, thus preventing a time-scale separation between photogeneration and relaxation dynamics. Similar considerations apply to the various Coulomb-induced phenomena: The strong modifications induced by Coulomb correlation on the optical response of low-dimensional semiconductors play a significant role on the phase-breaking relaxation dynamics as well. It is thus evident that any theoretical analysis of the optical response of semiconductor heterostructures must provide a proper description of both coherent and incoherent phenomena as well as of their mutual coupling on the same kinetic level.

ACKNOWLEDGMENTS

I am particularly grateful to Tilmann Kuhn for his essential contribution in understanding most of the ideas and concepts discussed in this topical review. I wish to thank Stephan W. Koch, Torsten Meier, and Peter Thomas, as well as Elisa Molinari, for their relevant contributions to the research activity reviewed in the paper. I am also grateful to Roberto Cingolani, Thomas Elsaesser, Alfred Leitenstorfer, and Peter E. Selbmann for stimulating and fruitful discussions.

This work was supported in part by the EC Commission through the Network "ULTRAFAST".

---

[1] J. Shah, *Ultrafast Spectroscopy of Semiconductors and Semiconductor Nanostructures* (Springer, Berlin, 1996).
[2] L. Allen, J.H. Eberly, *Optical Resonance and Two-Level Atoms* (Interscience, New York 1975).
[3] M. Sargent III, M.O. Scully, W.E. Lamb Jr., *Laser Physics* (Addison-Wesley, New York 1977).
[4] Y.R. Shen, *The Principles of Nonlinear Optics* (Wiley, New York 1984).
[5] M.D. Levenson, S.S. Kano, *Introduction to Nonlinear Laser Spectroscopy* (Academic, Boston 1988).
[6] P. Meystre, M. Sargent III, *Elements of Quantum Optics*, 2nd edn. (Springer, Berlin, Heidelberg 1991).
[7] D.L. Mills, *Nonlinear Optics* (Springer, Berlin, Heidelberg 1991).
[8] H. Haug and S.W. Koch, *Quantum Theory of the Optical and Electronic Properties of Semiconductors*, 3rd Edn. (World Scientific, Singapore 1994).
[9] W. Demtroeder, *Laser Spectroscopy*, 2nd edn. (Springer, Berlin, Heidelberg 1996).
[10] F. Henneberger, S. Schmitt-Rink, E.O. Göbel (eds.), *Optics of Semiconductor Nanostructures* (Akademie Verlag, Berlin 1993).
[11] R.T. Phillips (ed.) *Coherent Optical Processes in Semiconductors*, NATO ASI Series B: Physics, Vol. 30 (Plenum, New York 1994).
[12] E.L. Hahn, Phys. Rev. **80**, 580 (1950).
[13] N.A. Kurnit, I.D. Abella, and S.R. Hartmann, Phys. Rev. Lett. **13**, 567 (1964).
[14] I.D. Abella, N.A. Kurnit, and S.R. Hartmann, Phys. Rev. **141**, 391 (1966).
[15] J. Shah and R.C. C. Leite, Phys. Rev. Lett. **22**, 1304 (1969).
[16] C.V. Shank, R.L. Fork, R.F. Leheny, and J. Shah, Phys. Rev. Lett. **42**, 112 (1979).
[17] J. Shah, B. Deveaud, T.C. Damen, W.T. Tsang, A.C. Gossard, and P. Lugli, Phys. Rev. Lett. **59**, 2222 (1987).
[18] T. Elsaesser, J. Shah, L. Rota, and P. Lugli, Phys. Rev. Lett. **66**, 1757 (1991).
[19] R.G. Ulbrich, J.A. Kash, and J.C. Tsang, Phys. Rev. Lett. **62**, 949 (1989).
[20] C.L. Peterson and S.A. Lyon, Phys. Rev. Lett. **65**, 760 (1990).
[21] D.W. Snoke, W.W. Rühle, Y.-C. Lu, and E. Bauser, Phys. Rev. Lett. **68**, 990 (1992).
[22] J.L. Oudar, A. Migus, D. Hulin, G. Grillon, J. Etchepare, and A. Antonetti, Phys. Rev. Lett. **53**, 384 (1984).
[23] J.-P. Foing, D. Hulin, M. Joffre, M.K. Jackson, J.-L. Oudar, C. Tanguy, and M. Combescot, Phys. Rev. Lett. **68**, 110 (1992).
[24] A. Leitenstorfer, C. Fürst, A. Laubereau, W. Kaiser, G. Tränkle, and G. Weimann, Phys. Rev. Lett. **76**, 1545 (1996).

[25] S. Lutgen, R. Kaindl, M. Woerner, T. Elsaesser, A. Hase, H. Künzel, M. Gulia, D. Meglio, and P. Lugli, Phys. Rev. Lett. **77**, 3657 (1996).
[26] M. Joschko, M. Woerner, T. Elsaesser, E. Binder, T. Kuhn, R. Hey, H. Kostial, and K. Ploog, Phys. Rev. Lett. **78**, 737 (1997).
[27] C. Jacoboni and P. Lugli, *The Monte Carlo Method for Semiconductor Device Simulations* (Springer, Wien 1989).
[28] S.M. Goodnick and P. Lugli, in *Hot Carriers in Semiconductor Nanostructures: Physics and Applications*, edited by J. Shah (Academic, San Diego 1992), p. 191.
[29] F. Rossi, P. Poli, and C. Jacoboni, Semicond. Sci. Technol. **7**, 1017 (1992).
[30] A. Mysyrowicz, D. Hulin, A. Antonetti, A. Migus, W.T. Masselink, and H. Morkoç, Phys. Rev. Lett. **56**, 2748 (1986).
[31] N. Peyghambarian, S.W. Koch, M. Lindberg, B.D. Flügel, M. Joffre, Phys. Rev. Lett. **62**, 1185 (1989).
[32] W.H. Knox, D.S. Chemla, D.A.B. Miller, J.B. Stark, and S. Schmitt-Rink, Phys. Rev. Lett. **1989**, 1189 (1989).
[33] S.T. Kundiff, A. Knorr, J. Feldmann, S.W. Koch, E.O. Göbel, H. Nichel, Phys. Rev. Lett. **73**, 1178 (1994).
[34] P.C. Becker, H.L. Fragnito, C.H. Brito Cruz, R.L. Fork, J.E. Cunningham, J.E. Henry, and C.V. Shank, Phys. Rev. Lett. **61**, 1647 (1988).
[35] Y. Masumoto, S. Shionoya, and T. Takagahara, Phys. Rev. Lett. **51**, 923 (1983).
[36] L. Schultheis, J. Kuhl, A. Honold, and C.W. Tu, Phys. Rev. Lett. **57**, 1635 (1986); Phys. Rev. Lett. **57**, 1797 (1986).
[37] G. Noll, U. Siegner, S.G. Shevel, and E.O. Göbel, Phys. Rev. Lett. **64**, 792 (1990).
[38] V. Langer, H. Stolz, and W. von der Osten, Phys. Rev. Lett. **64**, 854 (1990).
[39] E.O. Göbel, K. Leo, T.C. Damen, J. Shah, S. Schmitt-Rink, W. Schäfer, J.F. Müller, and K. Köhler, Phys. Rev. Lett. **64**, 1801 (1990).
[40] D. Fröhlich, A. Kulik, B. Uebbing, A. Mysyrowicz, V. Langer, H. Stolz, and W. von der Osten, Phys. Rev. Lett. **67**, 2343 (1991).
[41] H. Stolz, V. Langer, E. Schreiber, S.A. Permogorov, W. von der Osten, Phys. Rev. Lett. **67**, 679 (1991).
[42] K. Leo, J. Shah, E.O. Göbel, T.C. Damen, S. Schmitt-Rink, W. Schäfer, and K. Köhler, Phys. Rev. Lett. **66**, 201 (1991).
[43] J. Feldmann, T. Meier, G. von Plessen, M. Koch, E.O. Göbel, P. Thomas, G. Bacher, C. Hartmann, H. Schweizer, W. Schäfer, and H. Nickel, Phys. Rev. Lett. **70**, 3027 (1993).
[44] C. Waschke, H.G. Roskos, R. Schwedler, K. Leo, H. Kurz, and K. Köhler, Phys. Rev. Lett. **70**, 3319 (1993).
[45] K. Leo, M. Wegener, J. Shah, D.S. Chemla, E.O. Göbel, T.C. Damen, S. Schmitt-Rink, and W. Schäfer, Phys. Rev. Lett. **65**, 1340 (1990).
[46] S. Weiss, M.-A. Mycek, J.-Y. Bigot, S. Schmitt-Rink, and D.S. Chemla, Phys. Rev. Lett. **69**, 2685 (1992).
[47] D.-S. Kim, J. Shah, J.E. Cunningham, T.C. Damen, W. Schäfer, M. Hartmann, and S. Schmitt-Rink, Phys. Rev. Lett. **68**, 1006 (1992).
[48] D.-S. Kim, J. Shah, T.C. Damen, W. Schäfer, F. Jahnke, S. Schmitt-Rink, and K. Köhler, Phys. Rev. Lett. **69**, 2725 (1992).
[49] H.G. Roskos, M.C. Nuss, J. Shah, K. Leo, D.A.B. Miller, A.M. Fox, S. Schmitt-Rink, and K. Köhler, Phys. Rev. Lett. **68**, 2216 (1992).
[50] P.C.M. Planken, M.C. Nuss, I. Brener, K.W. Goossen, M.S.C. Luo, S.L. Chuang, and L. Pfeiffer, Phys. Rev. Lett. **69**, 3800 (1992).
[51] C. Comte and G. Mahler, Phys. Rev.B **34**, 7164 (1986).
[52] S. Schmitt-Rink, C. Ell, and H. Haug, Phys. Rev. B**33**, 1183 (1986).
[53] S. Schmitt-Rink, D.S. Chemla, and H. Haug, Phys. Rev. B**37**, 941 (1988).
[54] K. Henneberger and H. Haug, Phys. Rev. B**38**, 9759 (1988).
[55] A.V. Kuznetsov, Phys. Rev. B**44**, 8721 (1991).
[56] H. Haug and C. Ell, Phys. Rev. B**46**, 2126 (1992).
[57] I. Balslev, R. Zimmermann, and A. Stahl, Phys. Rev. B**40**, 4095 (1989).
[58] S. Schmitt-Rink and D.S. Chemla, Phys. Rev. Lett. **57**, 2752 (1986).
[59] M. Lindberg and S.W. Koch, Phys. Rev. B**38**, 3342 (1988).
[60] M. Wegener, D.S. Chemla, S. Schmitt-Rink, and W. Schäfer, Phys. Rev. A**42**, 5675 (1990).
[61] W. Schäfer, F. Jahnke, and S. Schmitt-Rink, Phys. Rev. B**47**, 1217 (1993).
[62] E. Binder, T. Kuhn, and G. Mahler, Phys. Rev. **B50**, 18319 (1994).
[63] O. Hess and T. Kuhn, Phys. Rev. A **54**, 3347 (1996); ibid. 3360 (1996).
[64] T. Kuhn, in *Theory of Transport Properties of Semiconductor Nanostructures*, edited by E. Schöll (Chapman & Hall, London 1997).
[65] R.L. Fork, C.H. Brito Cruz, P.C. Becker, and C.V. Shank, Phys. Rev. Lett. **12**, 483 (1987).
[66] T. Kuhn and F. Rossi, Phys. Rev. Lett. **69**, 977 (1992).
[67] T. Kuhn and F. Rossi, Phys. Rev. B **46**, 7496 (1992).
[68] F. Rossi, S. Haas, and T. Kuhn, Semicond. Sci. Technol. **9**, 411 (1994).

[69] F. Rossi, S. Haas, and T. Kuhn, Phys. Rev. Lett. **72**, 152 (1994).
[70] S. Haas, F. Rossi, and T. Kuhn, Phys. Rev. B **53**, 12855 (1996).
[71] A. Lohner, K. Rick, P. Leisching, A. Leitenstorfer, T. Elsaesser, T. Kuhn, F. Rossi, and W. Stolz, Phys. Rev. Lett. **71**, 77 (1993).
[72] A. Leitenstorfer, A. Lohner, K. Rick, P. Leisching, T. Elsaesser, T. Kuhn, F. Rossi, W. Stolz, and K. Ploog, Phys. Rev. B **49**, 16372 (1994).
[73] A. Leitenstorfer, A. Lohner, T. Elsaesser, S. Haas, F. Rossi, T. Kuhn, W. Klein, G. Boehm, G. Traenkle, and G. Weimann, Phys. Rev. Lett. **73**, 1687 (1994).
[74] T. Kuhn, F. Rossi, A. Leitenstorfer, A. Lohner, T. Elsaesser, W. Klein, G. Boehm, G. Traenkle, and G.W. Weimann, in *Hot Carriers in Semiconductors*, edited by K. Hess, J.-P. Leburton, and U. Ravaioli (Plenum Press, New York, 1996), p. 199.
[75] A. Leitenstorfer, T. Elsaesser, F. Rossi, T. Kuhn, W. Klein, G. Boehm, G. Traenkle, and G.W. Weimann, Phys. Rev. B **53**, 9876 (1996).
[76] F. Bloch, Phys. Rev. **70**, 460 (1946).
[77] J.A. Kash and J.C. Tsang, in *Light Scattering in Solids VI*, edited by M. Cardona and G.Güntherodt, Springer, Berlin (1989), p. 423.
[78] W. Pötz and P. Kocevar, Phys. Rev. B **28**, 7040 (1983).
[79] W. Quade, E. Schöll, F. Rossi, and C. Jacoboni, Phys. Rev. B **50**, 7398 (1994).
[80] F. Rossi, R. Brunetti, and C. Jacoboni, in *Hot Carriers in Semiconductor Nanostructures: Physics and Applications*, edited by J. Shah (Academic Press inc., Boston, 1992), p. 153.
[81] R. Brunetti, C. Jacoboni, and F. Rossi, Phys. Rev. B **39**, 10781 (1989).
[82] D.B. Tran Thoai and H. Haug, Phys. Rev. B **47**, 3574 (1993).
[83] K.E. Sayed, L. Bànyai, and H. Haug, Phys. Rev. **B50**, 1541 (1994).
[84] J. Schilp, T. Kuhn, and G. Mahler, Phys. Rev. B **50**, 5435 (1994).
[85] V. Meden, C. Wöhler, j. Fricke, and K. Schönhammer, Phys. Rev. **B52**, 5624 (1995).
[86] M.G. Kane, K.W. Sun, and S.A. Lyon, Semicond. Sci. Technol. **9**, 697 (1994).
[87] J.A. Kash, Phys. Rev. **B51**, 4680 (1995).
[88] F. Bloch, Z. Phys. **52**, 555 (1928).
[89] C. Zener, Proc. R. Soc. **145**, 523 (1934).
[90] W.V. Houston, Phys. Rev. **57**, 184 (1940).
[91] E.O. Kane, J. Phys. Chem. Solids **12**, 181 (1959)
[92] P.N. Argyres, Phys. Rev. **126**, 1386 (1962).
[93] G.H. Wannier, Phys. Rev. **117**, 432 (1960).
[94] J. Zak, Phys. Rev. Lett. **20**, 1477 (1968).
[95] C. Kittel, *Quantum Theory of Solids* (Wiley, New York, 1963), p. 190.
[96] J.B. Krieger and G.J. Iafrate, Phys. Rev. B **33**, 5494 (1986).
[97] G. Nenciu, Rev. Mod. Phys. **63**, 91 (1991).
[98] G. Bastard, *Wave Mechanics of Semiconductor Heterostructures*, Les Editions de Physique (Les Ulis, France, 1989).
[99] E.E. Mendez, F. Agullo-Rueda, and J.M. Hong, Phys. Rev. Lett. **60**, 2426 (1988).
[100] P. Voisin, J. Bleuse, C. Bouche, S. Gaillard, C. Alibert, and A, Regreny, Phys. Rev. Lett. **61**, 1639 (1988).
[101] J. Feldmann, K. Leo, J. Shah, D.A.B. Miller, J.E. Cunningham, T. Meier, G. von Plessen, A. Schulze, P. Thomas, and S. Schmitt-Rink, Phys. Rev. B **46**, 7252 (1992).
[102] G. von Plessen and P. Thomas, Phys. Rev. B **45**, 9185 (1992).
[103] K. Leo, P.H. Bolivar, F. Brüggemann, R. Schwedler, Solid State Commun. **84**, 943 (1992).
[104] P. Leisching, P. Haring Bolivar, W. Beck, Y. Dhaibi, F. Bruggemann, R. Schwedler, H. Kurz, K. Leo, and K. Köhler, Phys. Rev. B **50**, 14389 (1994).
[105] T. Dekorsy, P. Leisching, K. Kohler, and H. Kurz, Phys. Rev. B **50**, 8106 (1994).
[106] T. Dekorsy, R. Ott, H. Kurz, and K. Kohler, Phys. Rev. B **51**, 17275 (1995).
[107] H.G. Roskos, C. Waschke, R. Schwedler, P. Leisching, Y. Dhaibi, H. Kurz, and K. Köhler, Superlattices and Microstructures **15**, 281 (1994).
[108] F. Rossi, in *Theory of Transport Properties of Semiconductor Nanostructures*, edited by E. Schöll (Chapman & Hall, London 1997).
[109] F. Rossi, T. Meier, P. Thomas, S.W. Koch, P.E. Selbmann, and E. Molinari, Phys. Rev. B **51**, 16943 (1995).
[110] F. Rossi, T. Meier, P. Thomas, S.W. Koch, P.E. Selbmann, and E. Molinari, in *Hot Carriers in Semiconductors*, edited by K. Hess, J.-P. Leburton, and U. Ravaioli (Plenum Press, New York, 1996), p. 157.
[111] T. Meier, F. Rossi, P. Thomas, and S.W. Koch, Phys. Rev. Lett. **75**, 2558 (1995).
[112] K.-C. Je, T. Meier, F. Rossi, and S.W. Koch, Appl. Phys. Lett. **67**, 2978 (1995).
[113] S.W. Koch, T. Meier, T. Stroucken, A. Knorr, J. Hader, F. Rossi, and P. Thomas, in *Microscopic theory of semiconductors: quantum kinetics, confinement and lasers*, edited by S.W. Koch (World Scientific, Singapore, 1995), p. 81.
[114] F. Rossi, M. Gulia, P.E. Selbmann, E. Molinari, T. Meier, P. Thomas, and S.W. Koch, in *Proc. 23rd ICPS,*

Berlin, Germany, edited by M. Scheffler and R. Zimmermann (World Scientific, Singapore, 1996), p. 1775.
[115] H. Rücker, E. Molinari, and P. Lugli, Phys. Rev. B **45**, 6747 (1992).
[116] E. Molinari, in *Confined Electrons and Photons: New Physics and Applications*, edited by E. Burstein and C. Weisbuch (Plenum, New York, 1994).
[117] G. von Plessen, T. Meier, J. Feldmann, E.O. Göbel, P. Thomas, K.W. Goossen, J.M. Kuo, and R.F. Kopf, Phys. Rev. B **49**, 14058 (1994).
[118] M.M. Dignam and J.E. Sipe, Phys. Rev. Lett. **64**, 1797 (1990).
[119] See e.g. *Proc. 4th Internat. Conf. on Optics of Excitons in Confined Systems*, Il Nuovo Cimento D vol. 17 (1995).
[120] For a review see: R. Cingolani and R. Rinaldi, Rivista Nuovo Cimento **16**, 1 (1993).
[121] T. Ogawa and T. Takagahara, Phys. Rev. **B43**, 14325 (1991).
[122] T. Ogawa and T. Takagahara, Phys. Rev. **B44**, 8138 (1991).
[123] F. Rossi and E. Molinari, Phys. Rev. Lett. **76**, 3642 (1996).
[124] F. Rossi and E. Molinari, Phys. Rev. **B53**, 16462 (1996).
[125] F. Rossi and E. Molinari, in *Proc. 23rd ICPS, Berlin, Germany*, edited by M. Scheffler and R. Zimmermann (World Scientific, Singapore, 1996), p. 1161.
[126] R. Rinaldi, R. Cingolani, M. Lepore, M. Ferrara, I.M. Catalano, F. Rossi, L. Rota, E. Molinari, P. Lugli, U. Marti, D. Martin, F. Morrier-Gemoud, P. Ruterana, and F.K. Reinhart, Phys. Rev. Lett. **73**, 2899 (1994).
[127] T. Someya, H. Akiyama, and H. Sakaki, Phys. Rev. Lett. **76**, 2965 (1996).

FIG. 1. Generation rate of electrons as a function of k at different times and densities. After Ref.[74].

FIG. 2. Calculated and measured band-to-acceptor spectra for different carrier densities. After Ref.[74].

FIG. 3. Full width at half maximum of the unrelaxed peak and the first and second phonon replica as a function of carrier density obtained from the calculated and measured spectra. The lines connecting the theoretical values are meant as guides to the eye. After Ref.[74].

FIG. 4. Schematic illustration of the field-induced coherent motion of an electronic wavepacket initially created at the bottom of a miniband. Here, the width of the miniband exceeds the LO-phonon energy E_{LO}, so that LO-phonon scattering is possible. After Ref.[117].

FIG. 5. Schematic representation of the transitions from the valence to the conduction band of a superlattice in the Wannier-Stark localization regime. After Ref.[44].

FIG. 6. Full Bloch-oscillation dynamics corresponding to a laser photoexcitation resonant with the first-miniband exciton. (a) Time evolution of the electron distribution as a function of $k_{\|}$. (b) Average kinetic energy, (c) current, and (d) THz-signal corresponding to the Bloch oscillations in (a).

FIG. 7. (a) Total THz-signals for eight different spectral positions of the exciting laser pulse: $1540, 1560, \ldots, 1680$ meV (from bottom to top). (b) Individual THz-signal of the electrons and holes in the different bands for a central spectral position of the laser pulse of 1640 meV. After Ref.[113].

FIG. 8. (a) Total THz-radiation as a function of time; (b) Incoherently-summed polarization as a function of time. After Ref.[114].

FIG. 9. Absorption spectra for various static applied electric fields for a $GaAs/Al_{0.3}Ga_{0.7}As$ superlattice (well (barrier) width 95 (15) Å). The vertical displacements between any two spectra is proportional to the difference of the corresponding fields. The Wannier-Stark transitions are labeled by numbers, the lower (higher) edge of the combined miniband by E_0 (E_1). After Ref.[113].

FIG. 10. Typical cross-section of V-grooved wires derived from TEM micrographs and used to define the confinement potential entering the 2D single-particle Schrödinger equation. The wire width along y at the apex of the V is about 10 nm. The dashed lines identify the region (about 70×25 nm), where single-particle and excitonic wavefunctions are localized. After Ref.[124].

FIG. 11. Linear-absorption spectra of realistic V-shaped quantum-wire structures obtained by including the first electron and hole subbands only. Solid line: Coulomb correlated (CC) result; Dashed line: free-carrier (FC) result. After Ref.[125].

FIG. 12. (a) OS ratio and DOS vs. excess energy; (b) electron-hole correlation function. After Ref.[125].

FIG. 13. Non-linear absorption spectra: (a) single-subband case; (b) realistic 12-subband case. After Ref.[125].

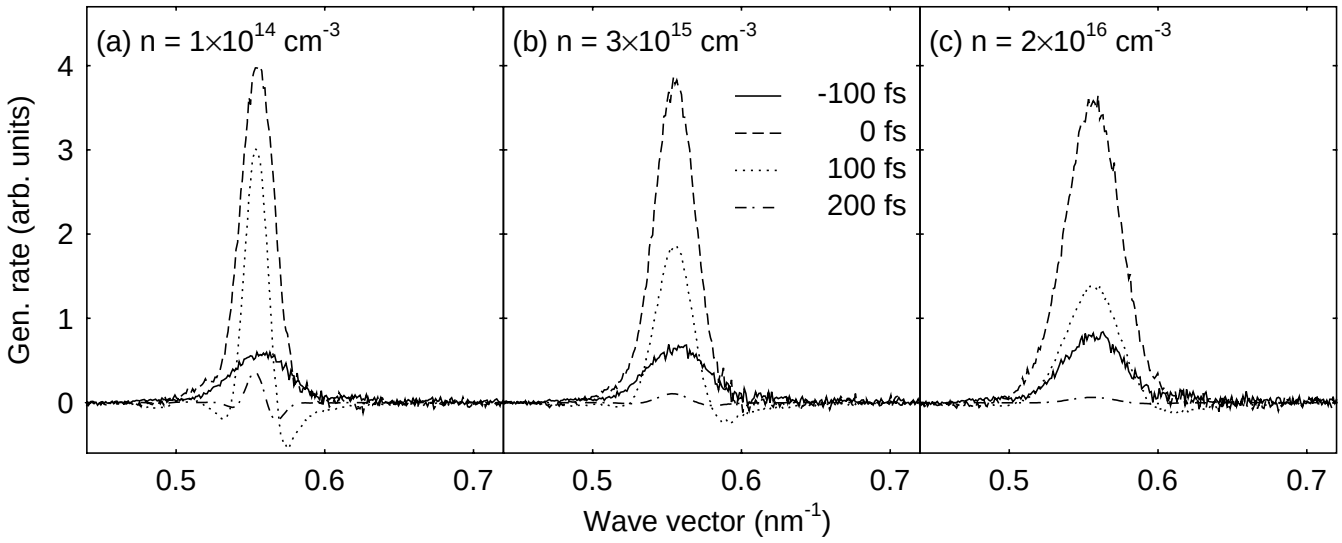
(a) n = 1×10^14 cm^-3
(b) n = 3×10^15 cm^-3
(c) n = 2×10^16 cm^-3
-100 fs
0 fs
100 fs
200 fs
Gen. rate (arb. units)
Wave vector (nm^-1)
0
1
2
3
4
0.5
0.6
0.7

F. Rossi, Fig. 1

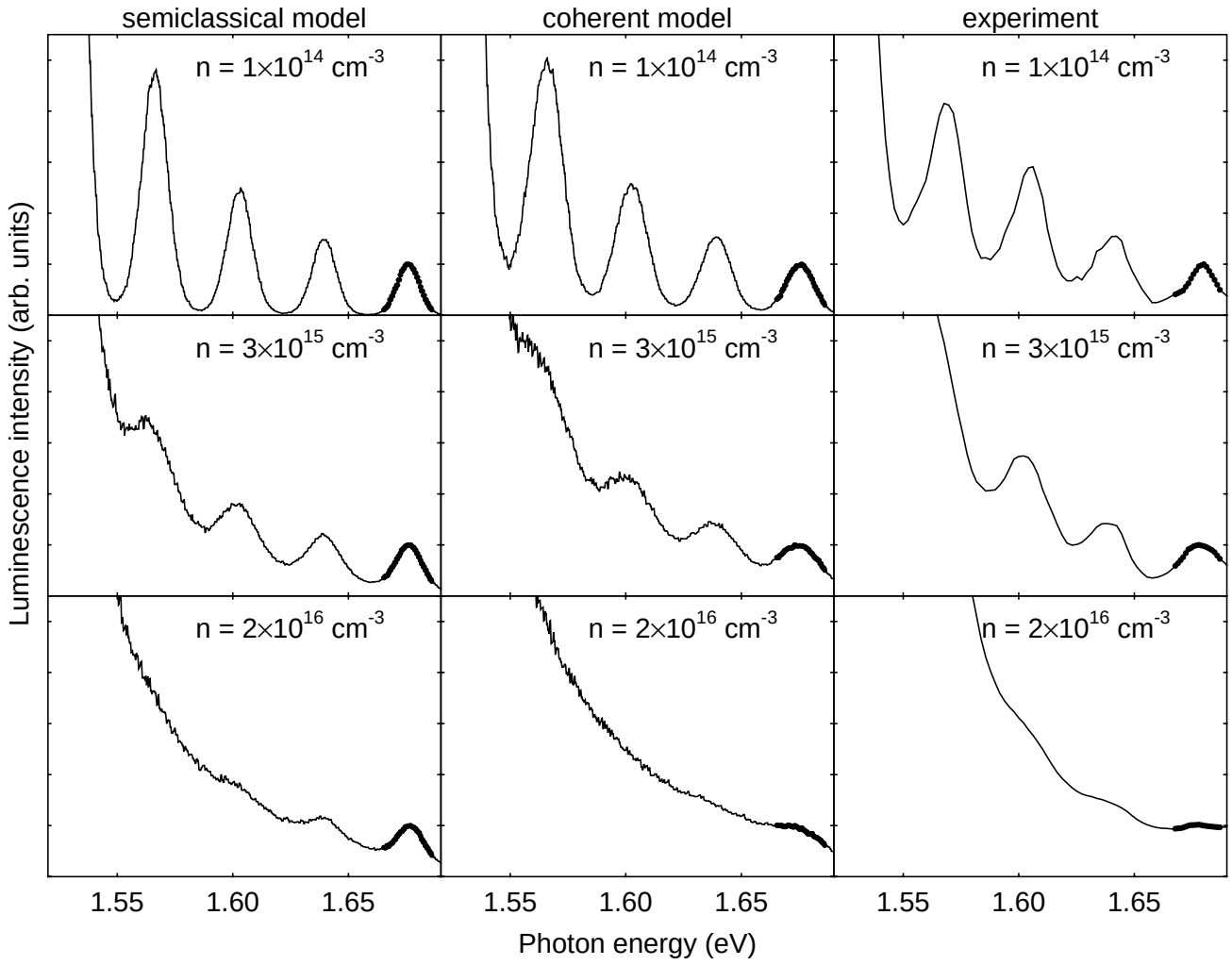
semiclassical model
coherent model
experiment
n = 1×10^14 cm^-3
n = 3×10^15 cm^-3
n = 2×10^16 cm^-3
Luminescence intensity (arb. units)
1.55
1.60
1.65
Photon energy (eV)

F. Rossi, Fig. 2

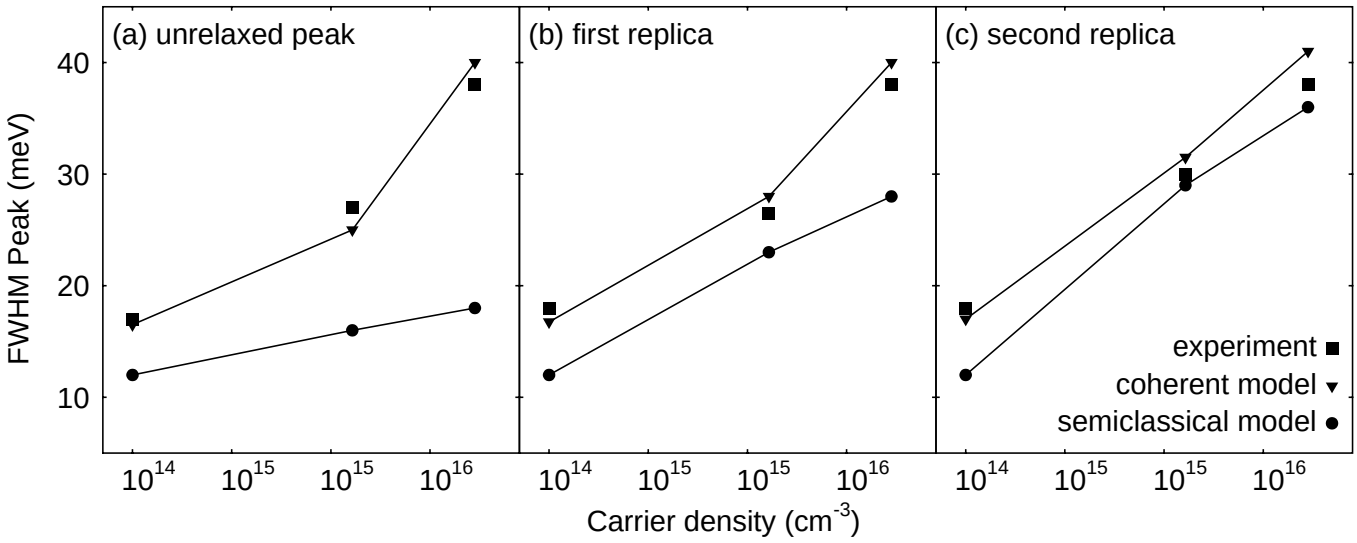
(a) unrelaxed peak
(b) first replica
(c) second replica
FWHM Peak (meV)
40
30
20
10
10^{14}
10^{15}
10^{15}
10^{16}
Carrier density (cm^{-3})
experiment
coherent model
semiclassical model

F. Rossi, Fig. 3

F. Rossi, Fig. 4

F. Rossi, Fig. 5

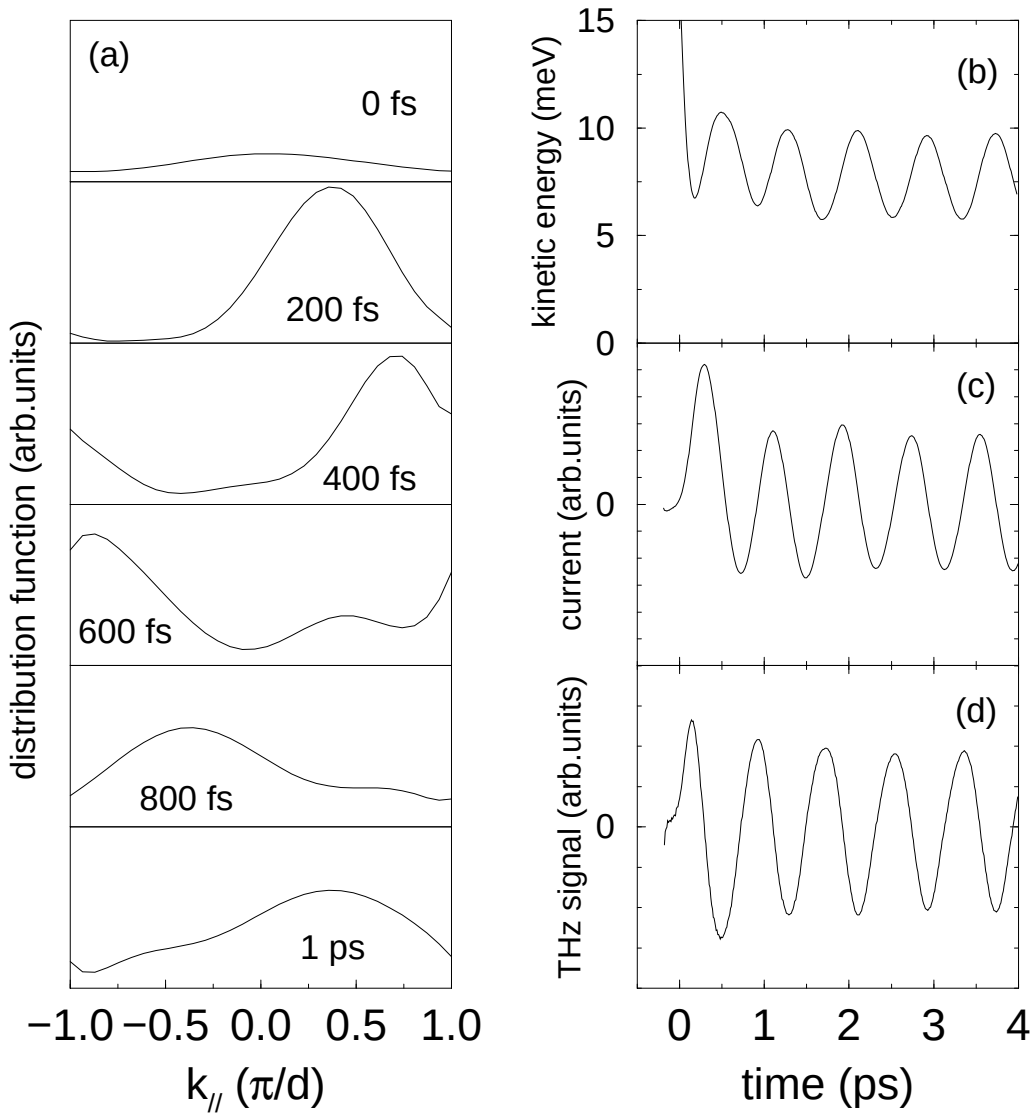
(a)
0 fs
200 fs
400 fs
600 fs
800 fs
1 ps
distribution function (arb.units)
−1.0 −0.5 0.0 0.5 1.0
k// (π/d)
(b)
kinetic energy (meV)
15
10
5
0
(c)
current (arb.units)
0
(d)
THz signal (arb.units)
0
0 1 2 3 4
time (ps)

F. Rossi, Fig. 6

F. Rossi, Fig. 7

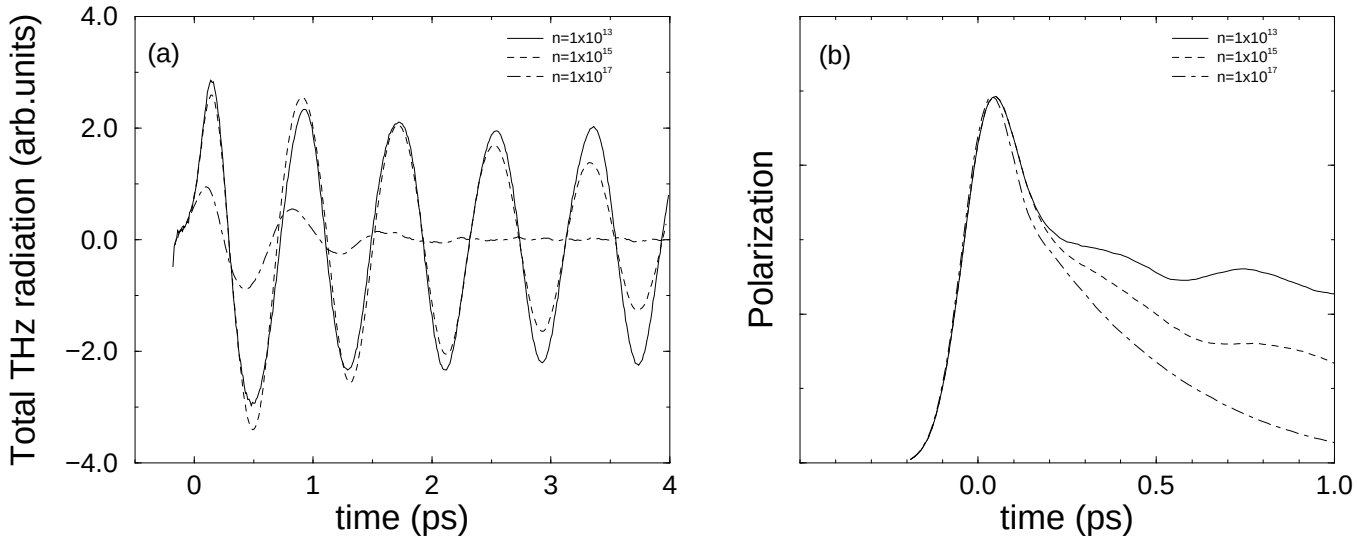
(a)
n=1x10^13
n=1x10^15
n=1x10^17
Total THz radiation (arb.units)
4.0
2.0
0.0
−2.0
−4.0
0
1
2
3
4
time (ps)
(b)
n=1x10^13
n=1x10^15
n=1x10^17
Polarization
0.0
0.5
1.0
time (ps)

F. Rossi, Fig. 8

F. Rossi, Fig. 9

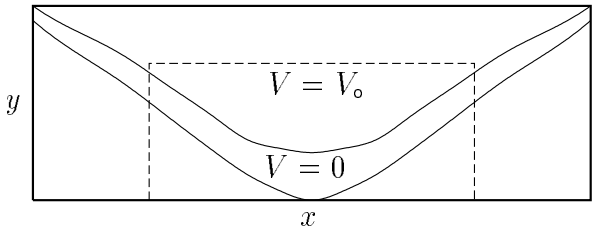

F. Rossi, Fig. 10

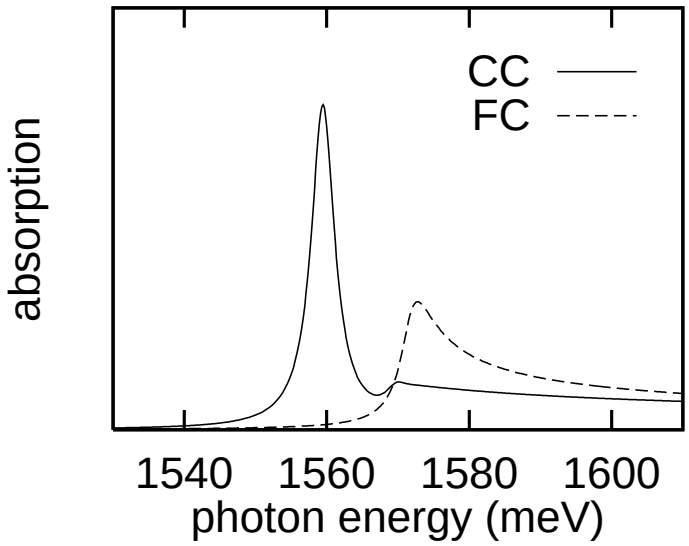

F. Rossi, Fig. 11

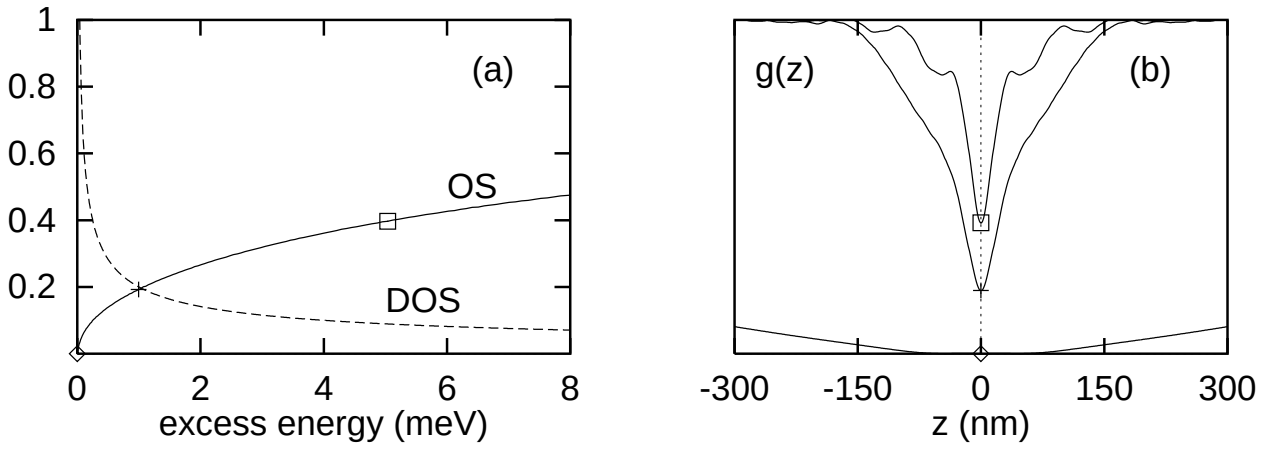

F. Rossi, Fig. 12

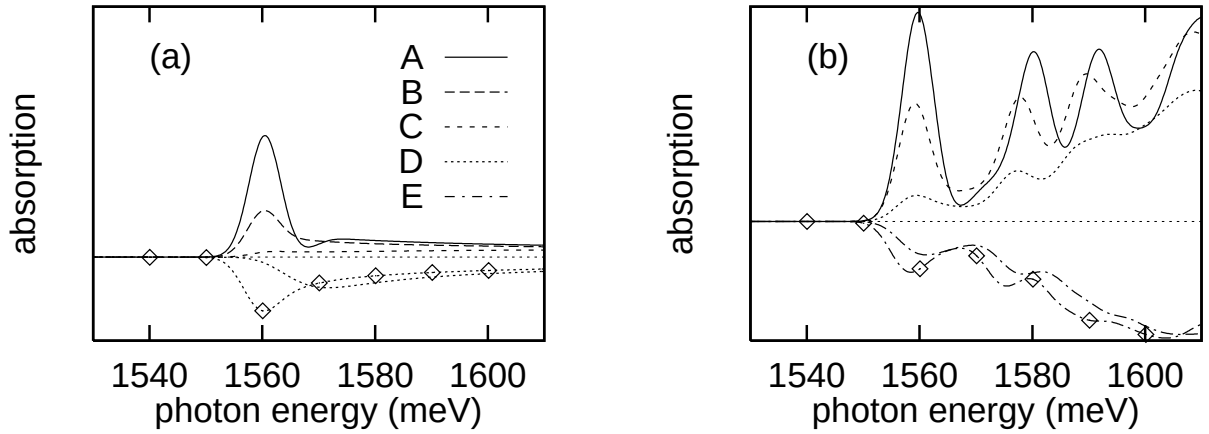

F. Rossi, Fig. 13